Dark Matter

ASTR 333/433

TODAY

Laws of Galactic Rotation

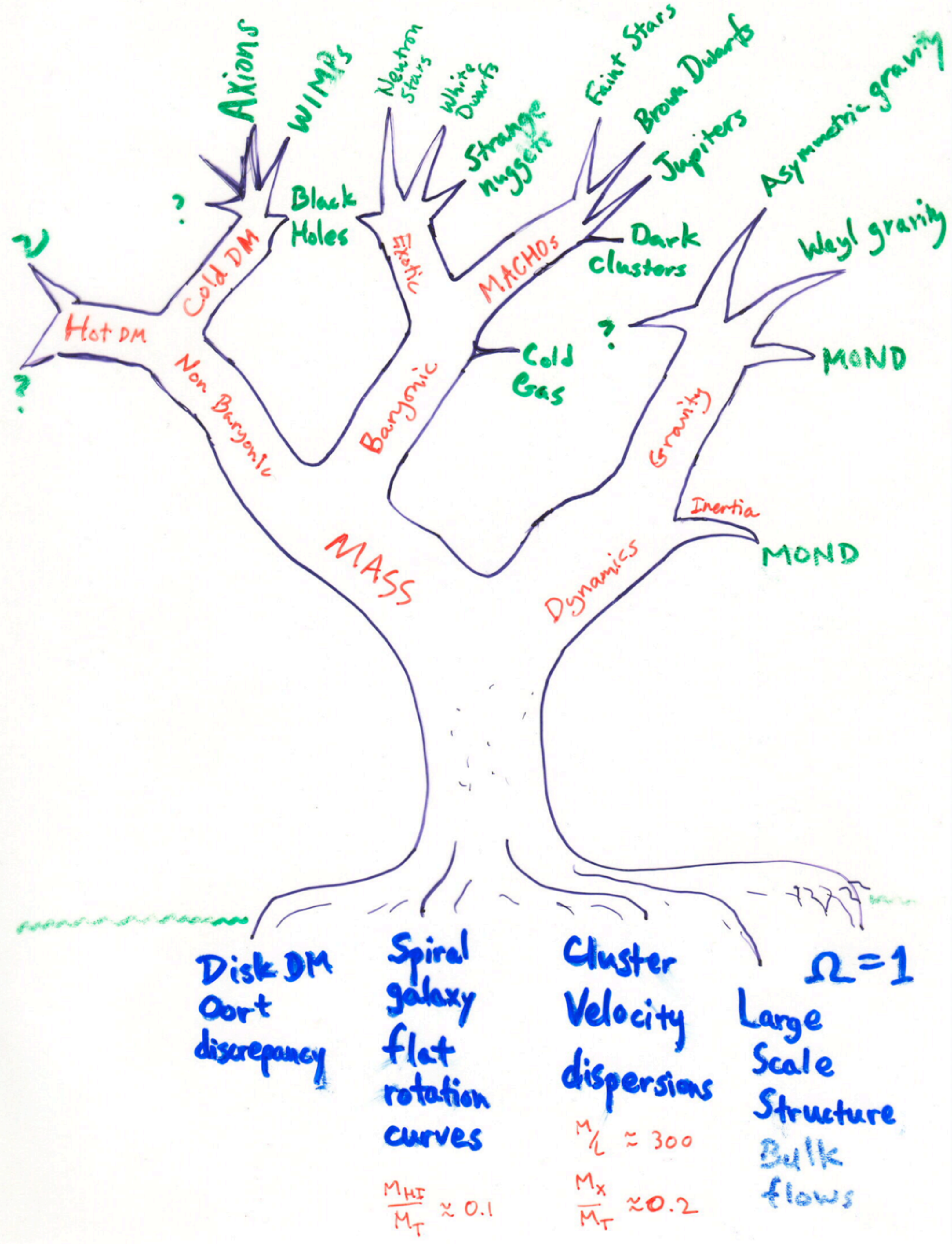

Empirical Laws of Galactic Rotation

- Flat rotation curves (Rubin-Bosma Law)

  Rotation curves tend asymptotically towards a constant rotation velocity that persists to indefinitely large radii: $V(R \to \infty) \to V_f$

- Tully-Fisher relation (Luminous, Stellar Mass, and Baryonic TF relations)

  The baryonic mass of galaxies scales as the fourth power of the flat rotation velocity: $M_b = AV_f^4$

- Central density relation (lower surface brightness galaxies exhibit larger mass discrepancies)

  The central dynamical surface densities of galaxies is related to their central surface brightnesses: $\Sigma_{dyn}(R \to 0) = f[\Sigma_*(R \to 0)]$

- Renzo's rule (Sancisi's Law)

  "For any feature in the luminosity profile there is a corresponding feature in the rotation curve and vice versa." (Sancisi 2004).

- Radial acceleration relation

  The observed centripetal acceleration is related to that predicted by the observed distribution of baryons: $\mathrm{g_{obs}} = \mathcal{F}(\mathrm{g_{bar}})$

Rotation curve amplitude depends on the mass of stars and gas (BTFR)

Rotation curve shape depends on the distribution of stars and gas

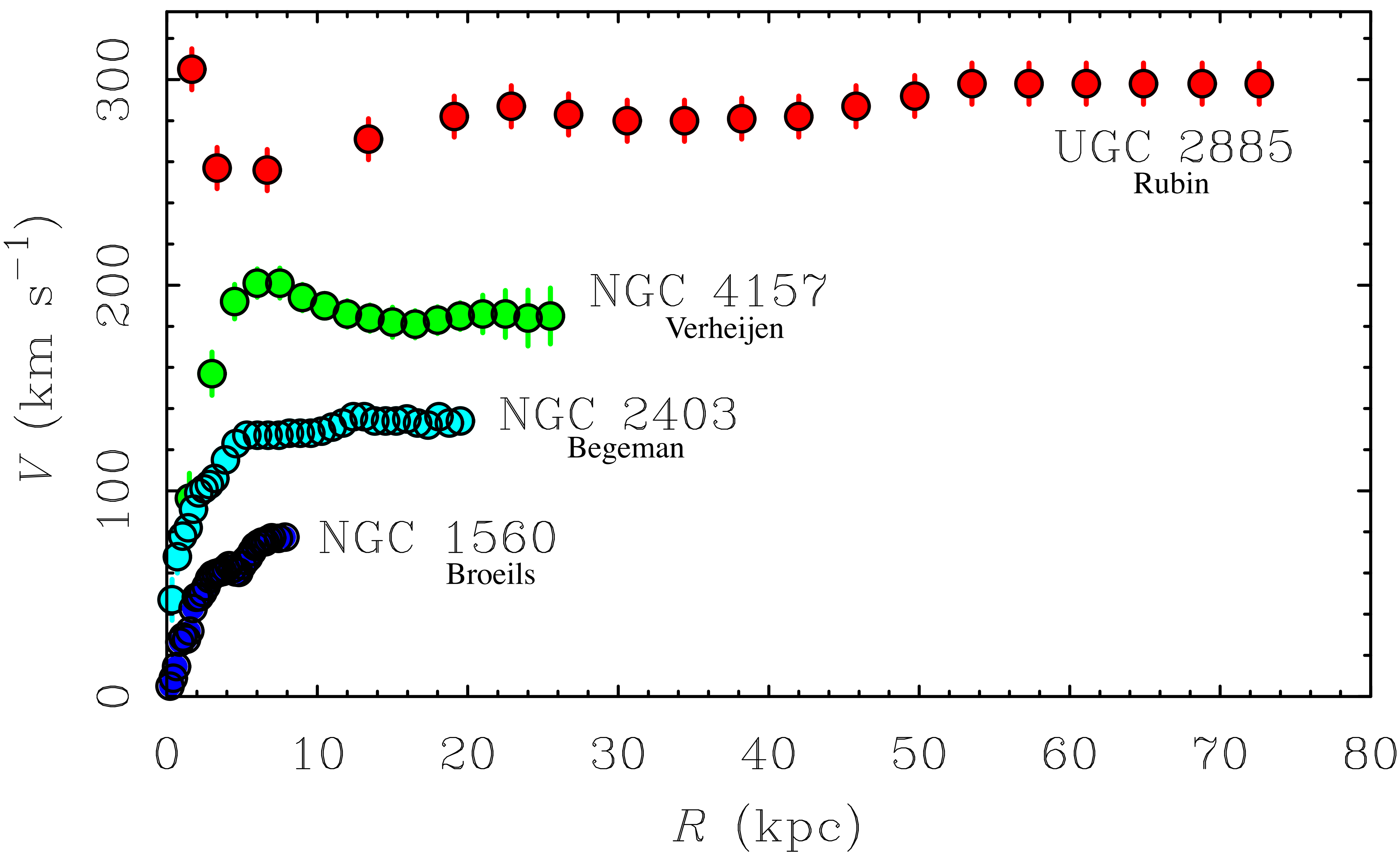

only near the limits of the optical image ($\kappa \approx 1$); velocities of highest-luminosity Sc's reach 100 km s^{-1} in less than 1% of the optical radius ($\kappa < 0.01$). The plot of log κ versus log V_{max} (Fig. 3) emphasizes that κ is a reliable estimator of V_{max} and, hence, of absolute magnitude. Ignoring resolution effects for the most distant galaxies, this diagram is distance independent. Furthermore, a comparison of Figures 1 and 2 shows that the (log κ, M_B) relation is similar in form and scatter to the (log V_{max}, M_B) relation, i.e., the conventional TF relation. The choice of 100 km s^{-1} as a fiducial mark in measuring κ is not particularly critical to the success of the (log κ, M_B) relation, although it should be located beyond local nuclear effects so as to relate to the overall rotation curve. It should not be affected by nonaxisymmetric barlike motions and local velocity perturbations often observed at small nuclear distances.

From our published rotation curves, it is clear that an adopted measure could be chosen from a fairly wide range of velocities up to and including, of course, the velocity peak. Any one of such measures would serve as a luminosity discriminant. Thus the relationships exhibited in Figures 1 and 2 are representative of a family of dynamical-luminosity relationships. The family of such measures will be explored in detail in a future paper.

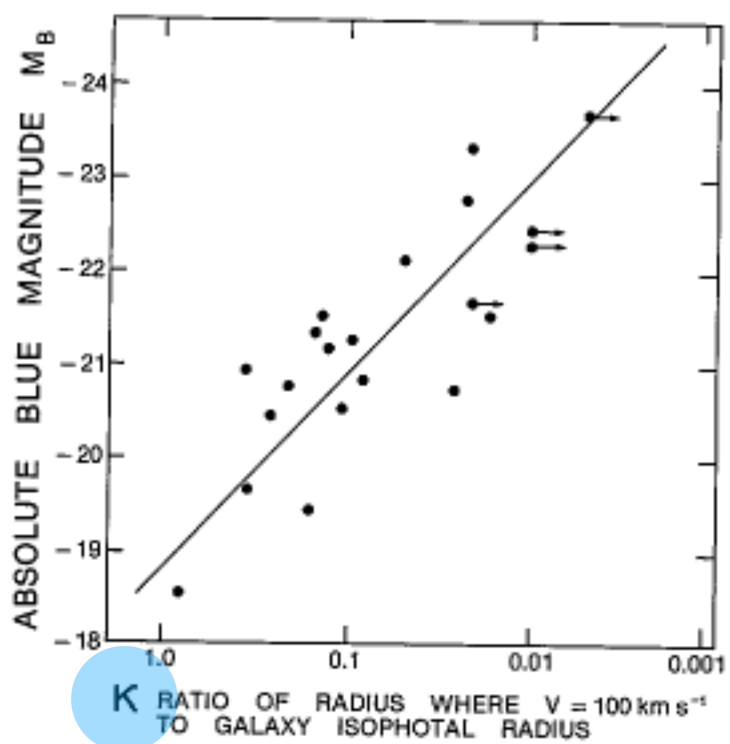

FIG. 2.—The correlation of M_B with log κ, the radial distance in the galaxy where the rotational velocity equals 100 km s^{-1}, in units of the isophotal radius. For lowest-luminosity Sc galaxies, the rotational velocity reaches 100 km s^{-1} only near the limits of the optical image ($\kappa \approx 1$), while for high-luminosity Sc's, the rotational velocity reaches 100 km s^{-1} in less than 1% of the optical radius ($\kappa < 0.01$).

nical scale and in Figure 4b scaled to the size of the galaxy. At every radial distance r in the constant-

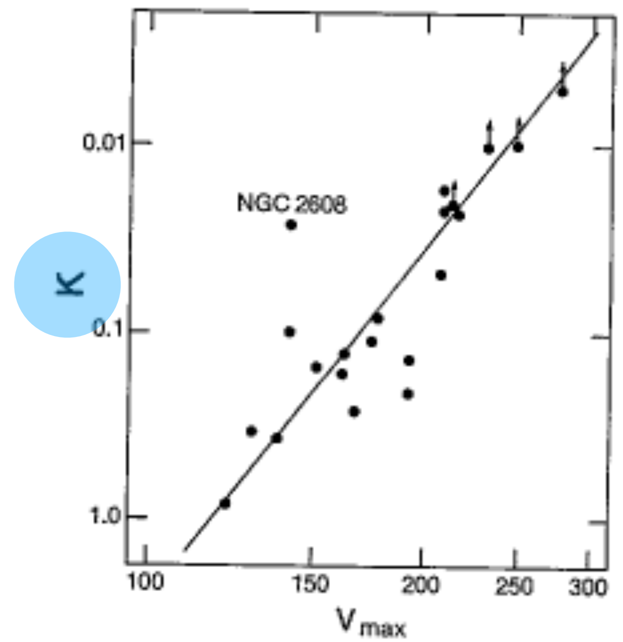

FIG. 3.—The correlation of log κ, the radius where the rotational velocity equals 100 km s^{-1} in units of the isophotal radius, vs. log V_{max}. The line is the mean of the two regressions and has a slope equal to 6.3 ± 0.5. NGC 2608, the only strongly barred galaxy in the sample, was excluded from the solution.

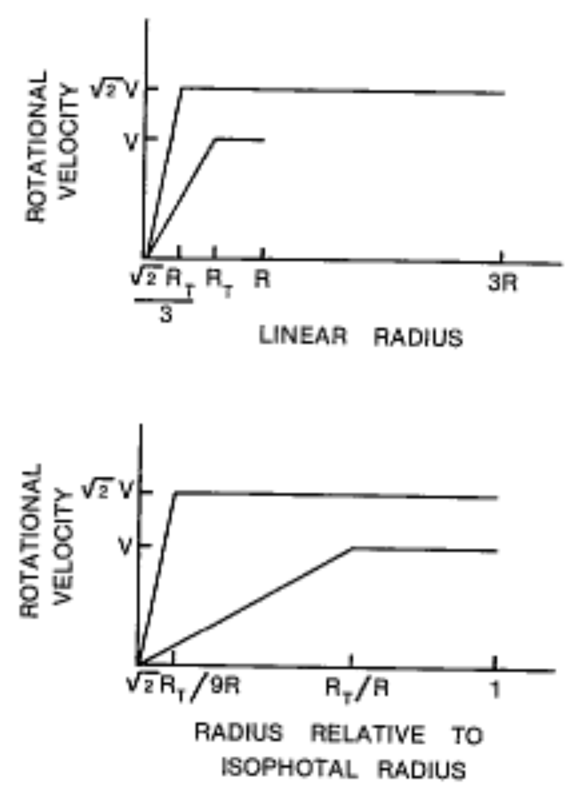

FIG. 4.—Schematic rotation curves for two Sc galaxies on a linear (*upper*) and relative (*lower*) radius scale. The higher-luminosity galaxy is chosen to have its velocity in the flat portion √(2) times that of the lower-luminosity galaxy. Then the nuclear velocity gradient, turnover radius, and radial extent are fixed by the observations as shown (see text and Table 2).

known for a long time

Rotation curve *shapes* correlate with galaxy properties

Rubin et al. 1980, *ApJ*, **242**, L149

κ here is the radius where $V(R/R_{isophotal}) = 100$ km/s. This is small in bright galaxies, which have steeply rising rotation curves, and large in dim galaxies, which have slowly rising rotation curves.

known for a long time

Rotation curve *shapes* correlate with galaxy properties

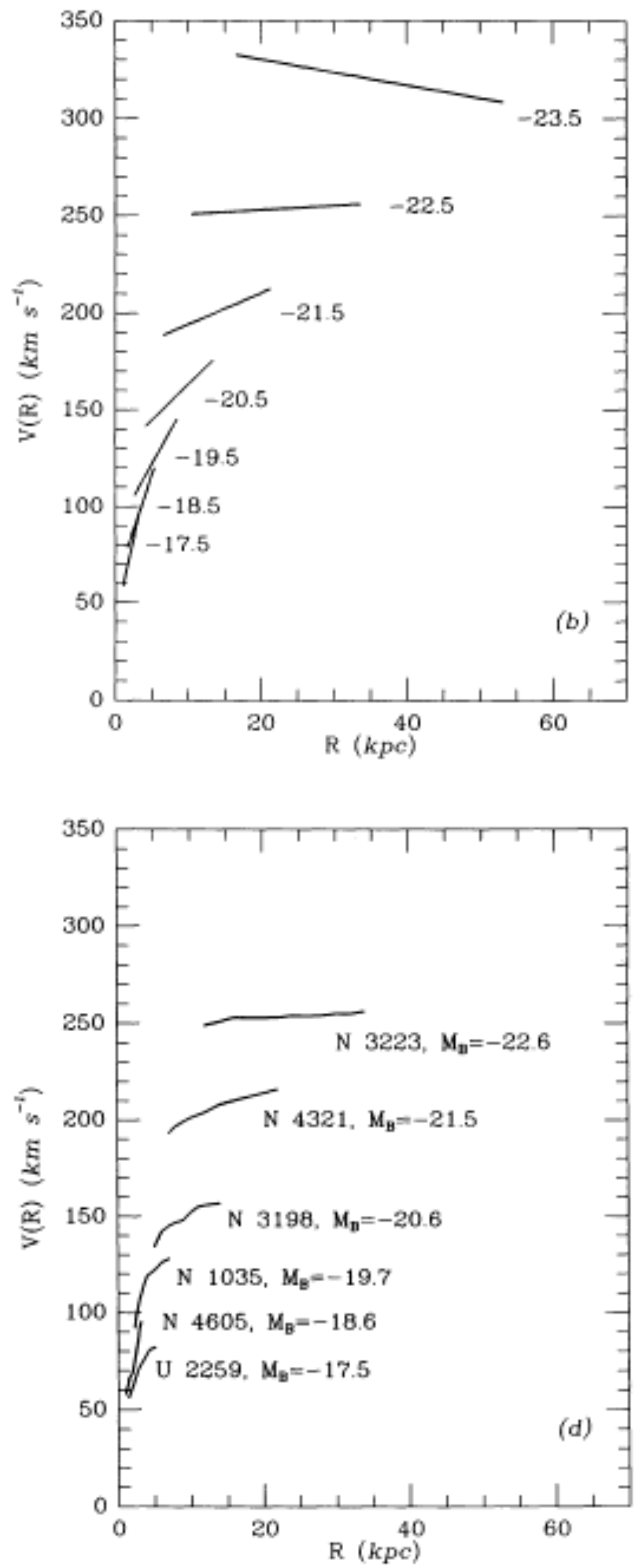

Persic & Salucci 1991
“Universal Rotation Curve”

Depends on both the luminosity and the scale length… turns out that surface brightness is the key quantity.

Rotation curve shape correlates with baryonic surface density

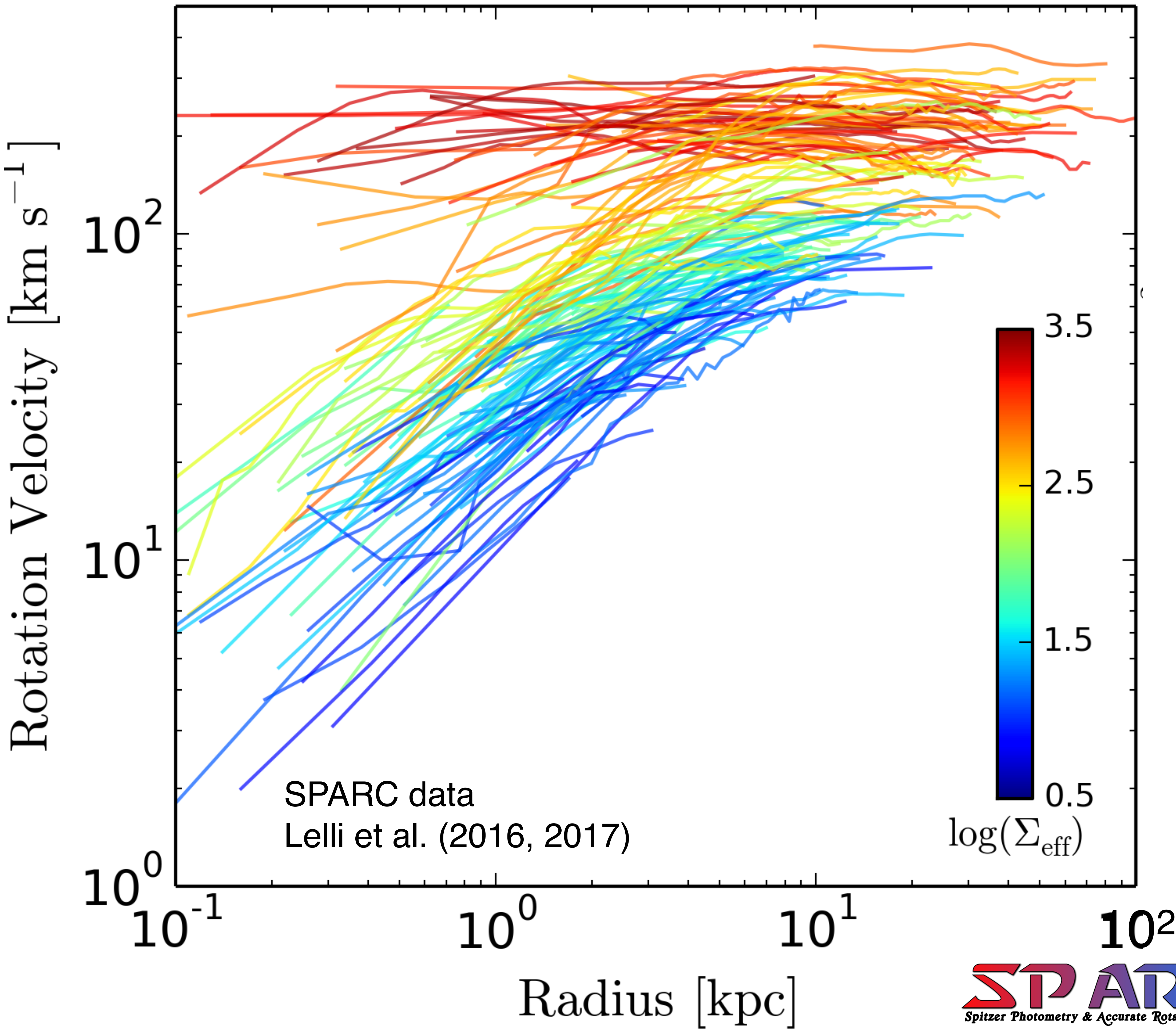

Spitzer Photometry & Accurate Rotation Curves

Remember our TF pair?

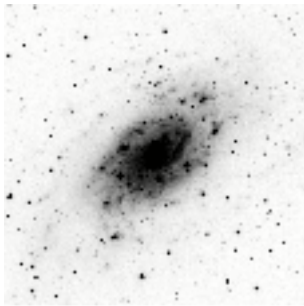

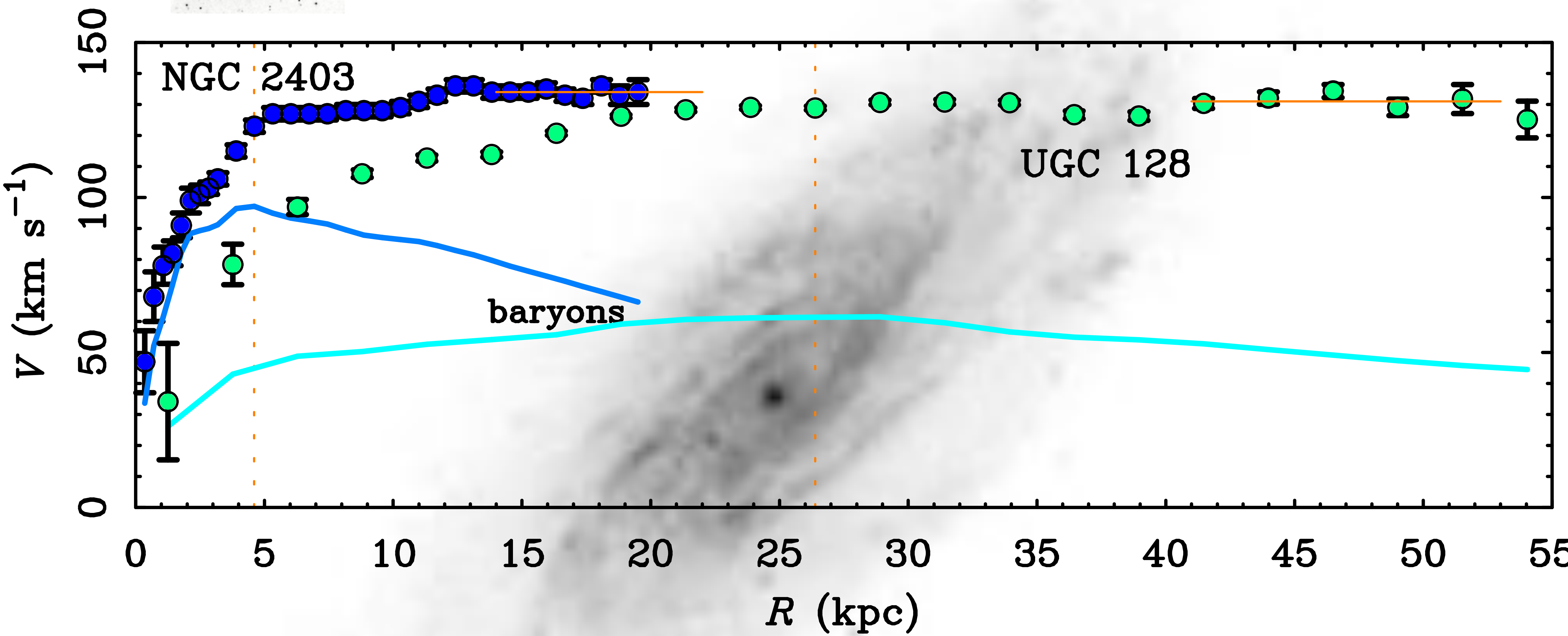

Radius in physical units (kpc)

Persic & Salucci 1996
de Blok & McGaugh 1996
Tully & Verheijen (1998)
Nordermeer & Verheijen (2007) [URC nor quite right formulation]
Swaters et al. (2009)

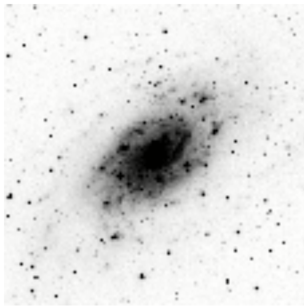

The dynamics knows about the distribution of baryons, not just their total mass

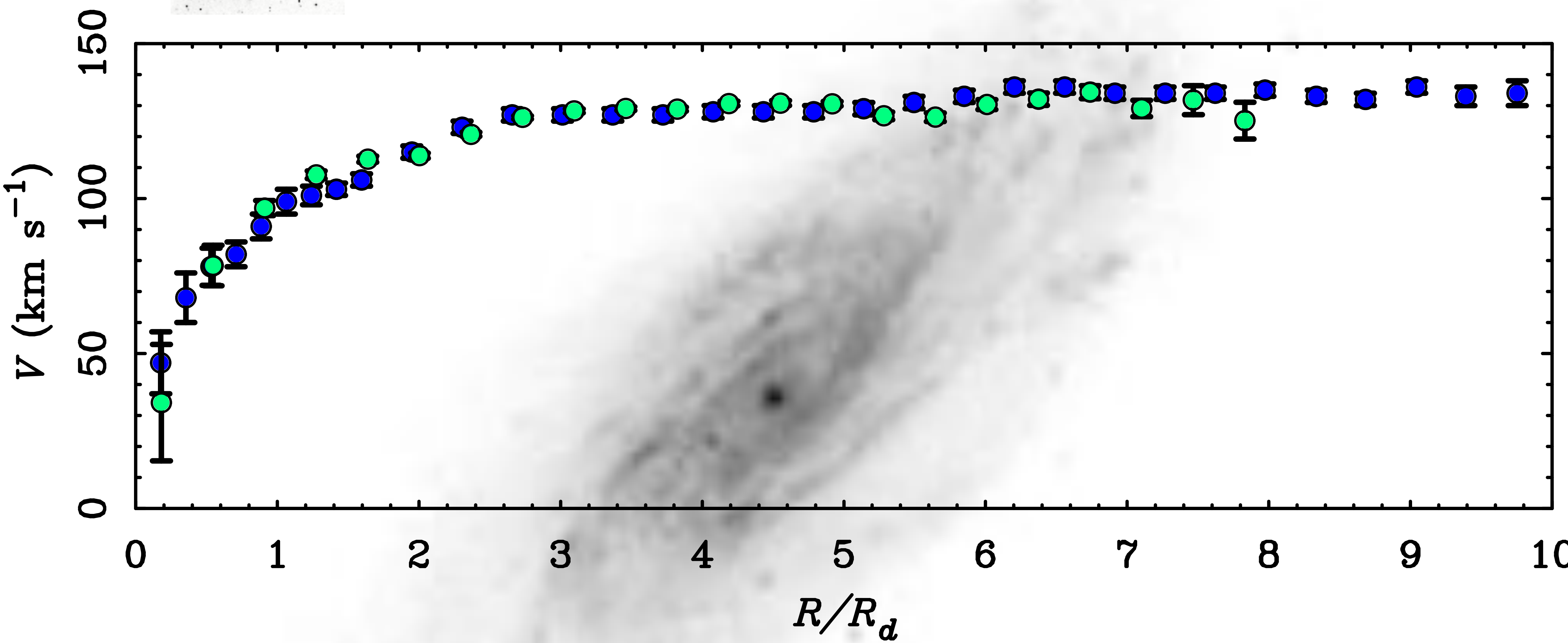

Radius normalized by size of disk.

Persic & Salucci 1996
de Blok & McGaugh 1996
Tully & Verheijen (1998)
Nordermeer & Verheijen (2007) [URC nor quite right formulation]
Swaters et al. (2009)

Rotation curve shape correlates with baryonic surface density

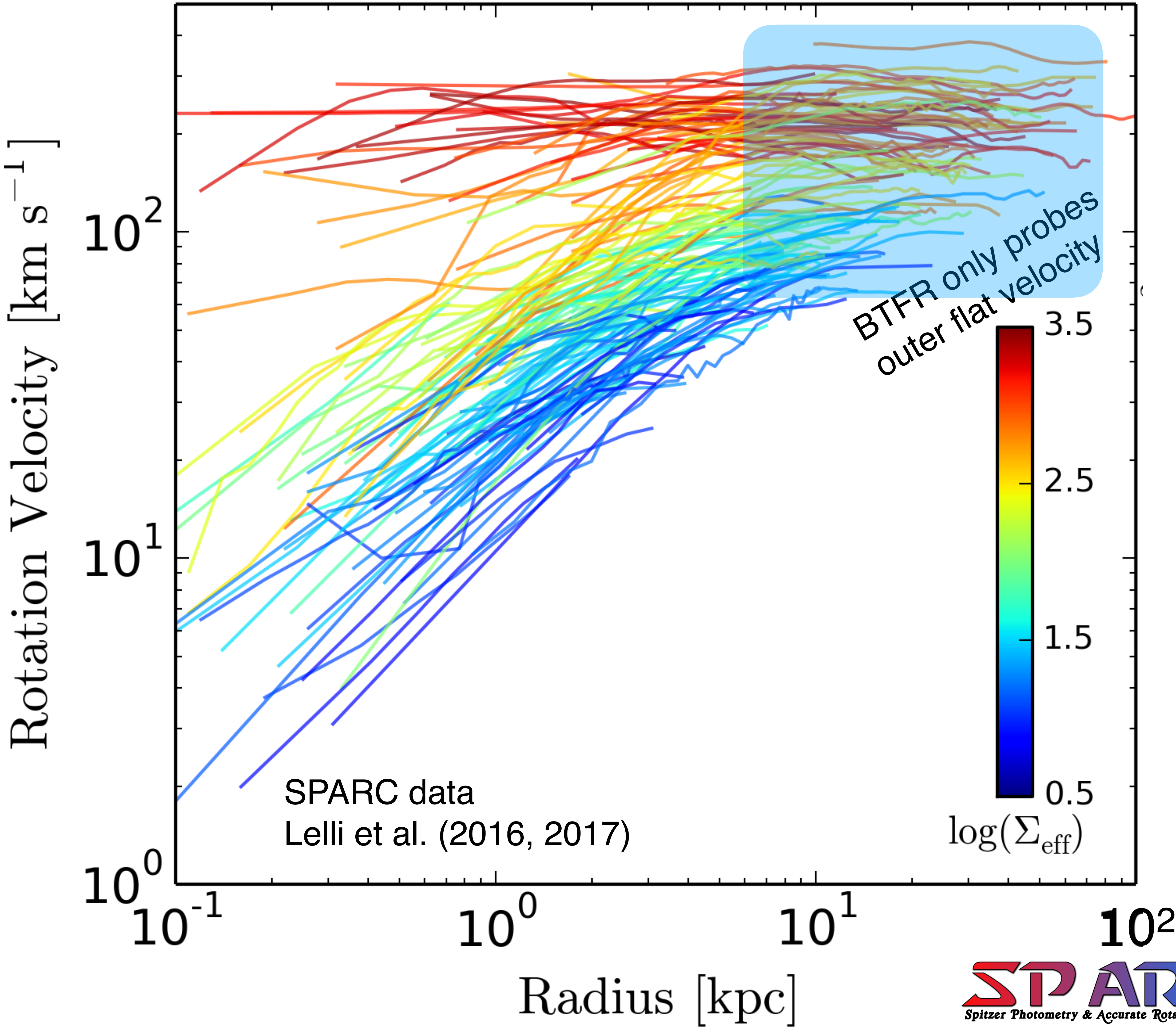

SPARC Spitzer Photometry & Accurate Rotation Curves

Rotation curve shape correlates with baryonic surface density

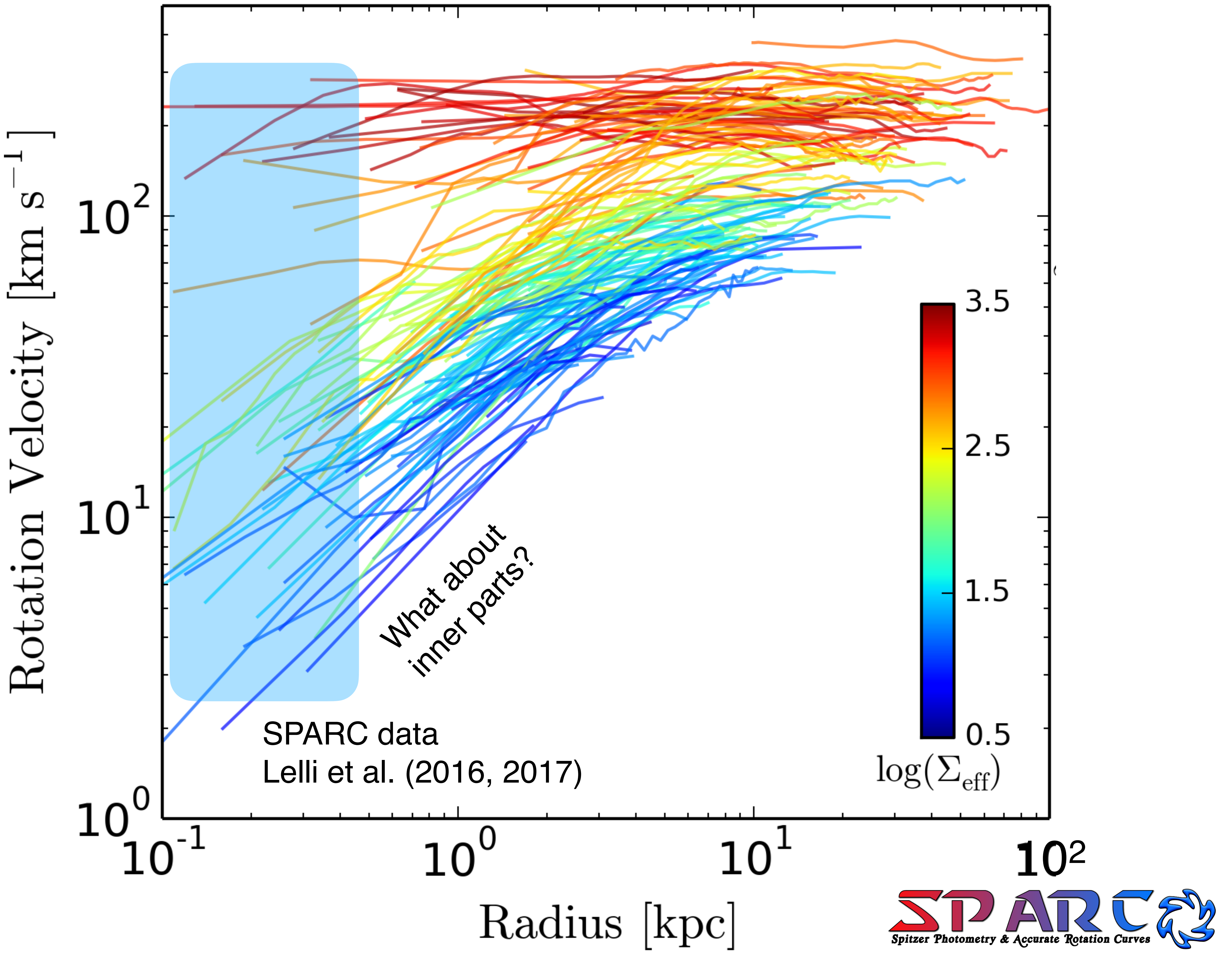

Central Density Relation

Lelli et al. (2016)

The *dynamical* central mass surface density correlates with the central surface brightness of stars in galaxies.

central dynamical surface density

Toomre (1963)

$$\Sigma_{dyn}(0) = \frac{1}{2\pi G}\int_0^\infty \frac{V^2(R)}{r^2}dR$$

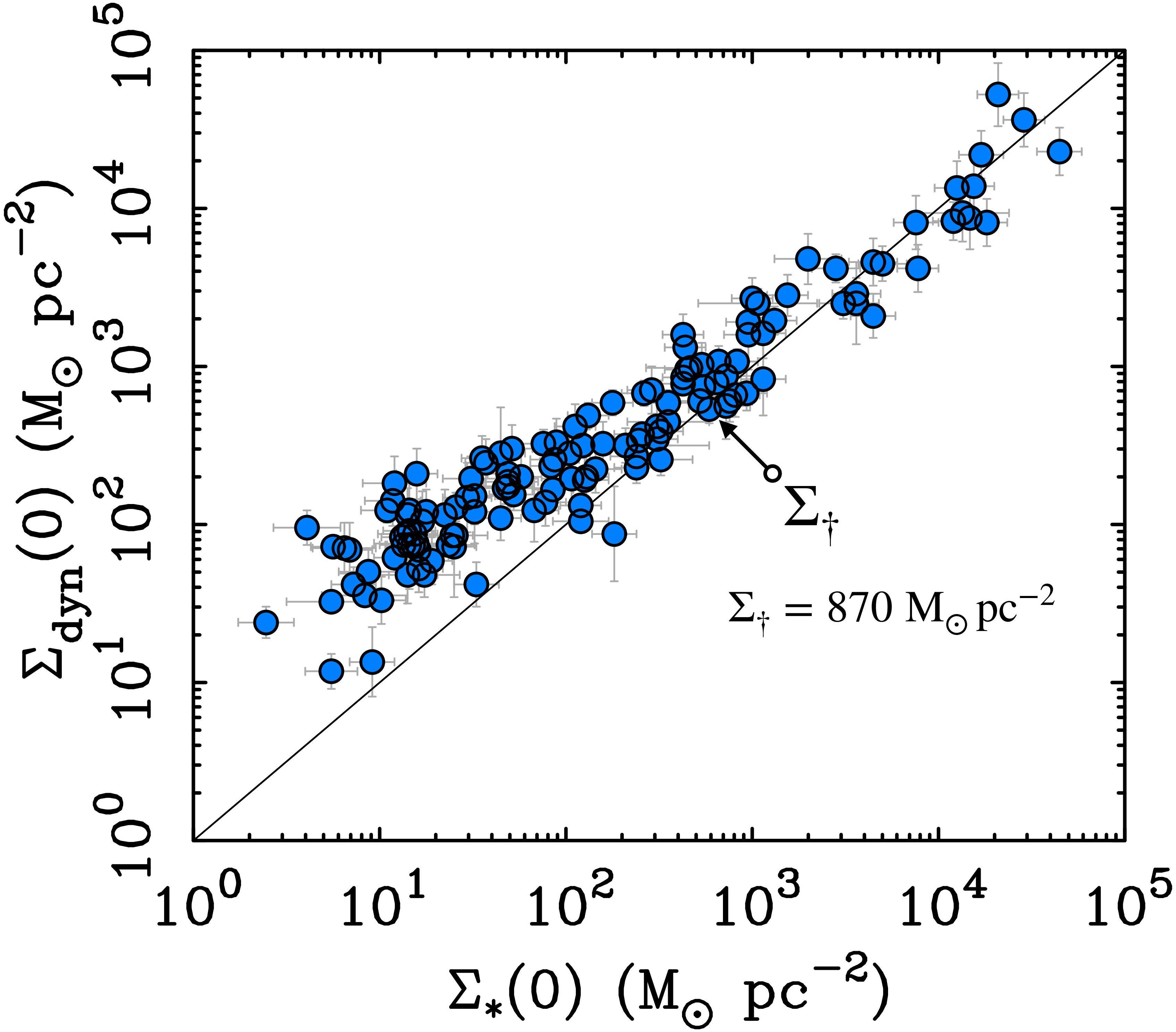

central surface brightness

Dynamical central mass surface density $\Sigma_{dyn}(R=0)$:

$$\Sigma_{dyn}(0) = \frac{1+q_0}{2\pi G}\int_0^\infty \frac{V^2}{R^2}dR$$

q_0 is the disk thickness: $q_0 \approx 0.15$

$$\Sigma_{dyn}(0) = \frac{1}{2\pi}\Sigma_\dagger f(y) \qquad y = \frac{\Sigma_*(0)}{2\pi\Sigma_\dagger}$$

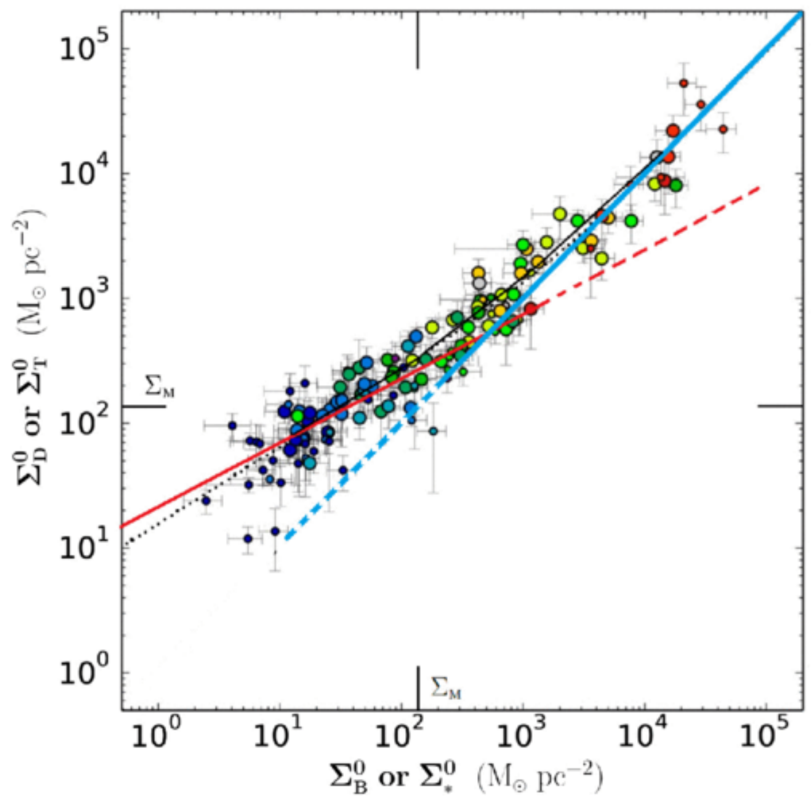

$$f(y) = \frac{y}{2} + y^{1/2}\left(1+\frac{y}{4}\right)^{1/2} + 2\sinh\left(\frac{y^{1/2}}{2}\right)$$

Asymptotically,

$\Sigma_{dyn}(0) \to \Sigma_*(0)$ for $\Sigma_*(0) \gg \Sigma_\dagger$ linear at high surface density

$\Sigma_{dyn}(0) \to \left(\frac{1}{\pi}\Sigma_\dagger\Sigma_*(0)\right)^{1/2}$ for $\Sigma_*(0) \ll \Sigma_\dagger$ square root at low surface density

What you get depends on how you look at it: what you assume & what you choose to measure:

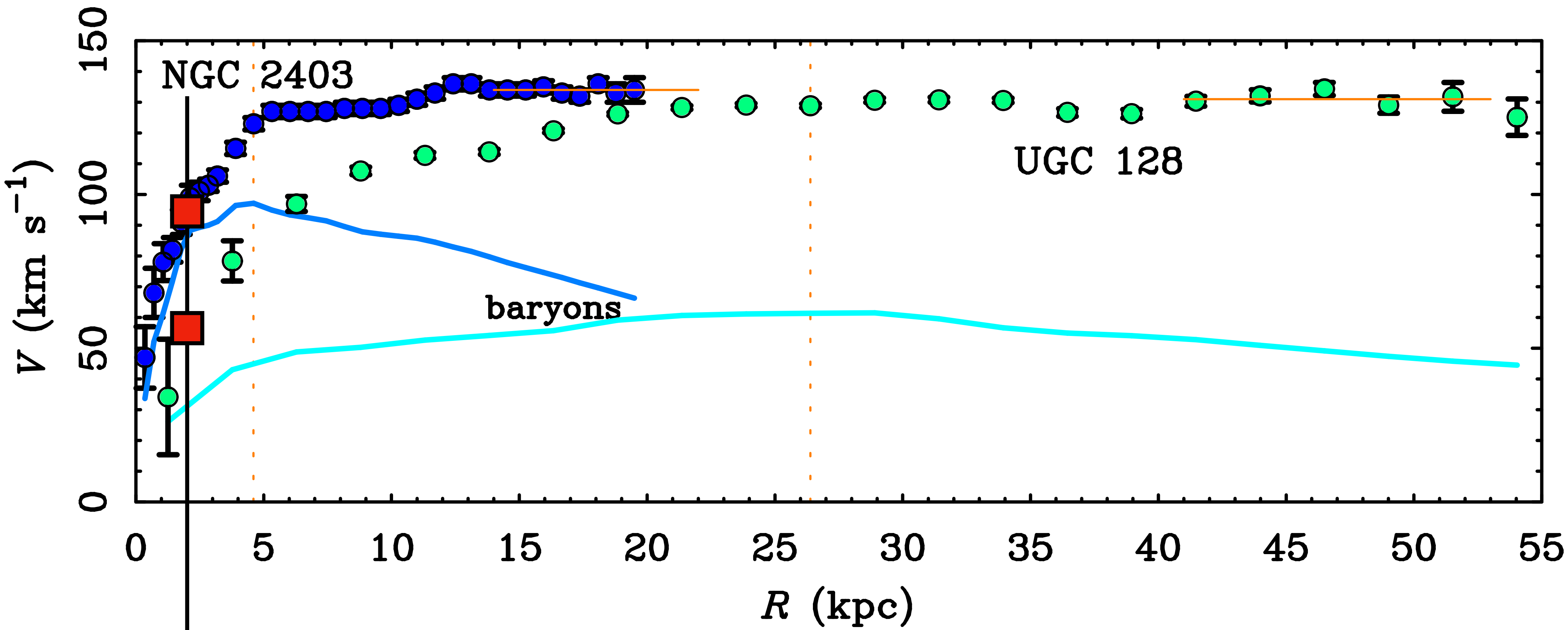

If you measure V(R in kpc) you infer **diversity**.

If you measure V(R in scale lengths) you infer **uniformity**.

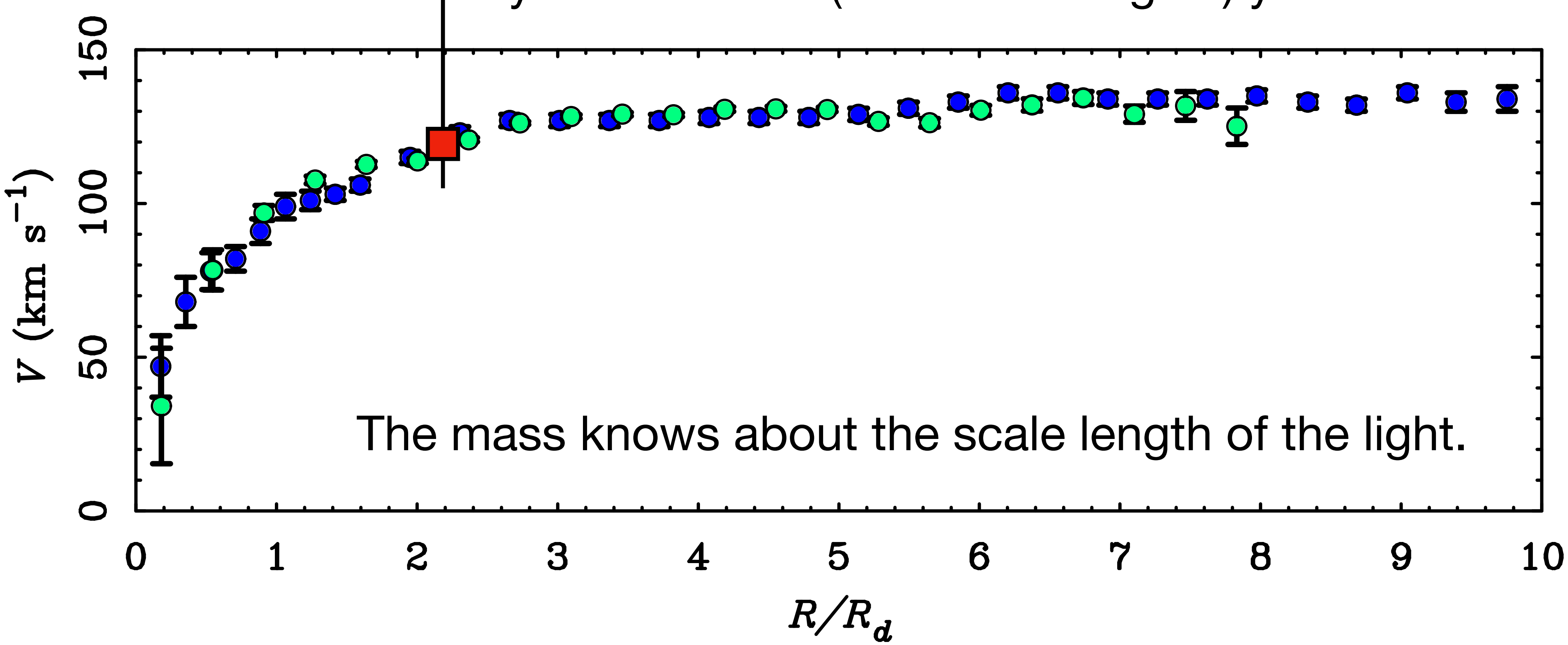

- Renzo's Rule: (2004 IAU; 1995 private communication) *"When you see a feature in the light, you see a corresponding feature in the rotation curve."*

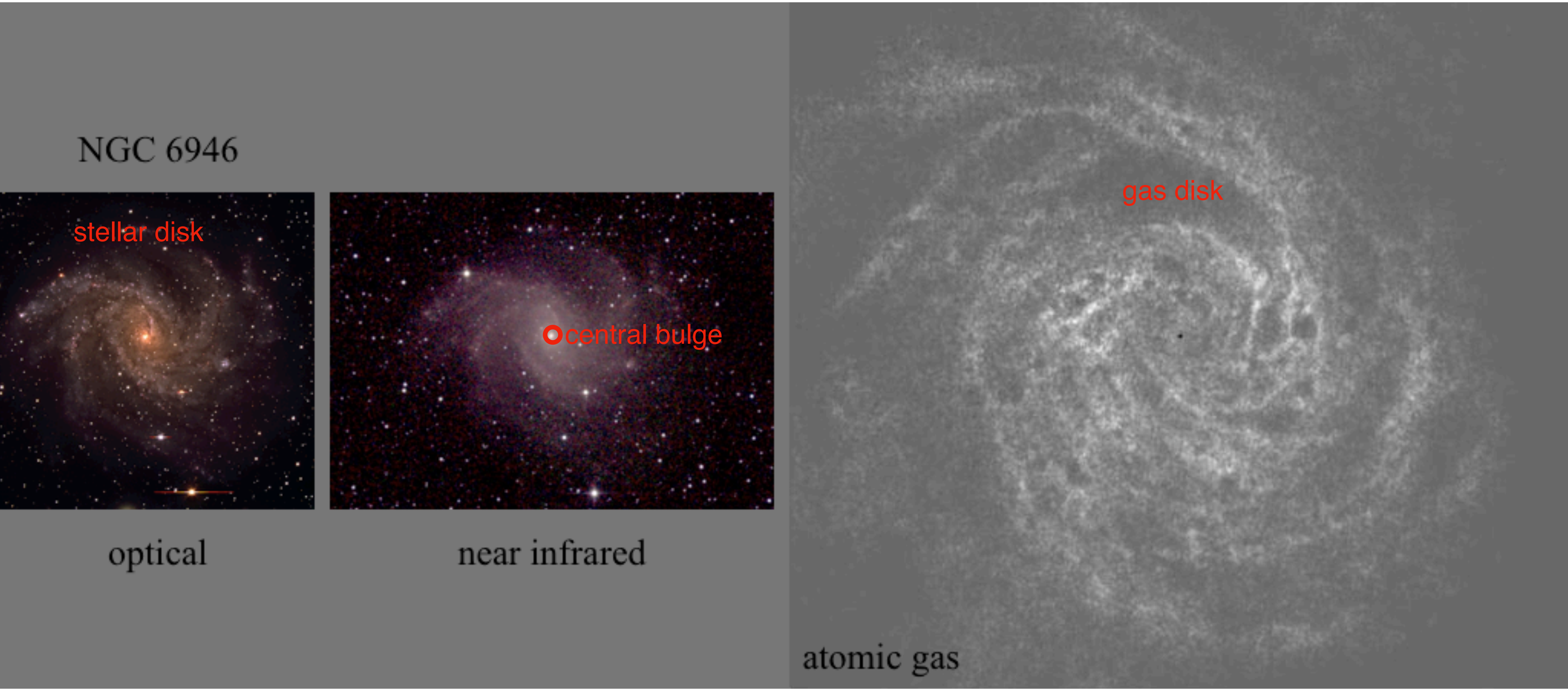

The central bulge component of NGC 6946 is only 6% of the total light, but it has a perceptible effect on the kinematics.

Note the up-down-up morphology - this requires a maximal bulge; can’t explain that with a dark matter halo.

V^2 = GM/R

M is small
but so is **R**

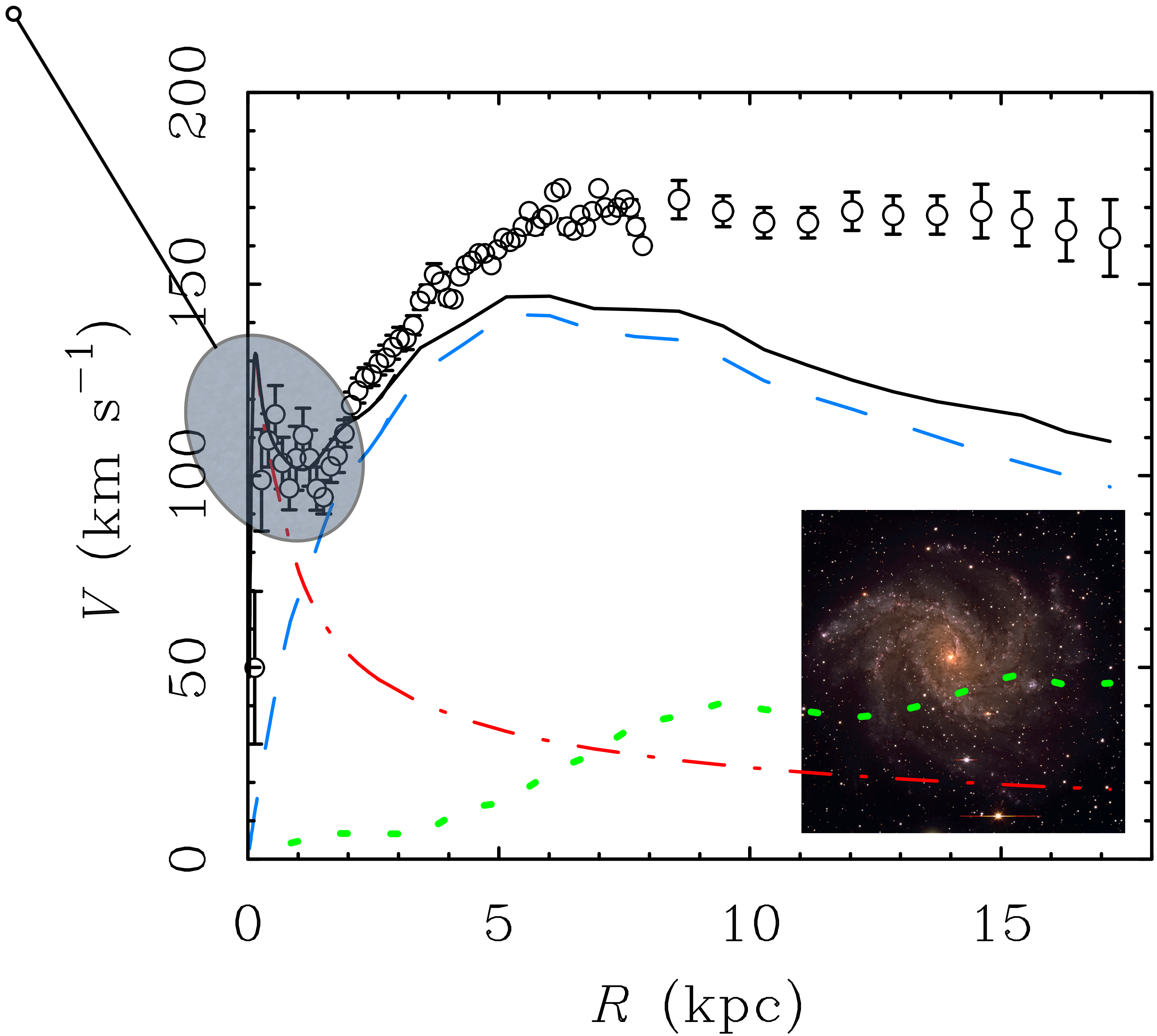

Renzo's Rule:

"When you see a feature in the light, you see a corresponding feature in the rotation curve."

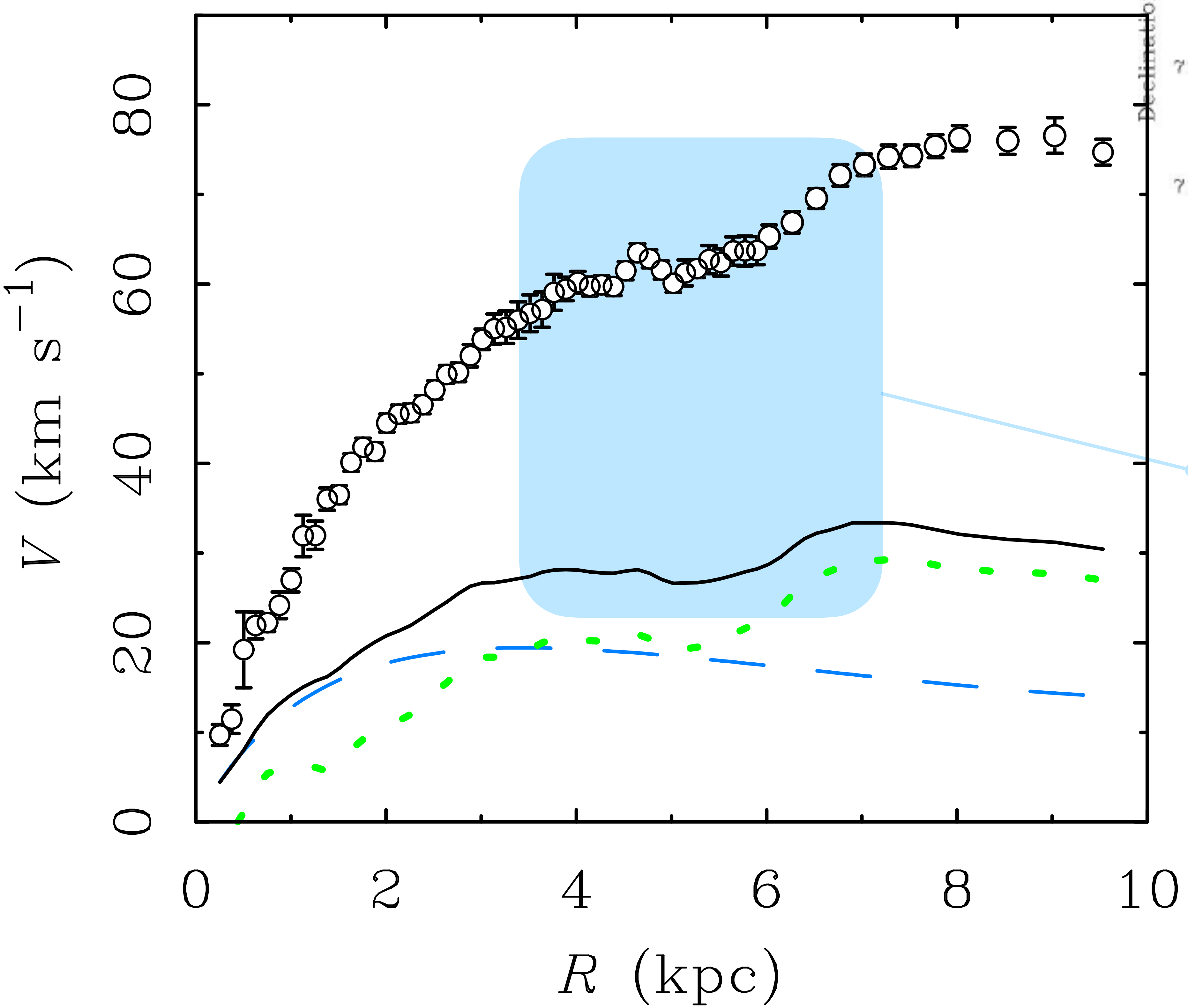

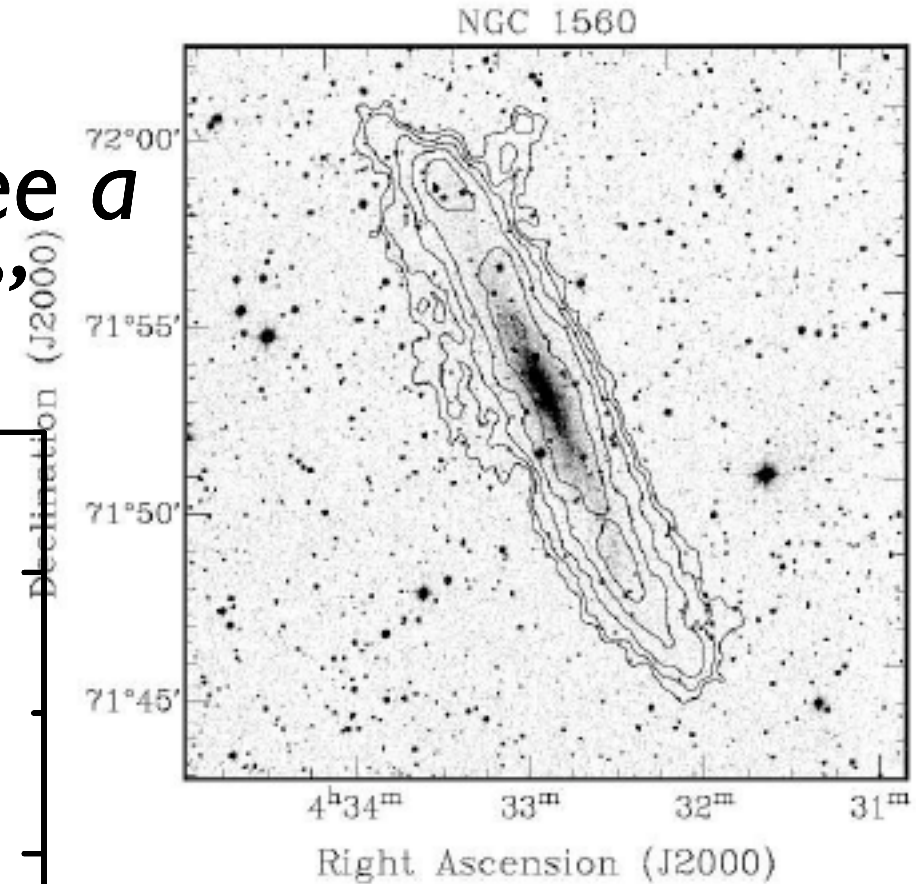

Gentile et al. (2010)

In NGC 1560, a marked feature in the gas is reflected in the kinematics, even though it accounts for little of the dynamical mass.

Mass models for baryonic components

$$V_b^2(r) = V_{bulge}^2(r) + \underbrace{V_{disk}^2(r)}_{\text{depends on } M_*/L} + V_{gas}^2(r)$$

- Bulge
  - not always spherical; sometimes more bar-like
- Stellar Disk
  - exponential a crude approximation
  - in practice, solve numerically for the observed surface brightness profile with DISKFIT or ROTMOD (in GIPSY)
- Gas disk
  - usually just HI; CO tracks stars

$$g_{\rm bar} = \frac{V_b^2}{R}$$

Now have

Surface density for
  stars
  gas
and corresponding rotation curves for each component

Observed rotation curve

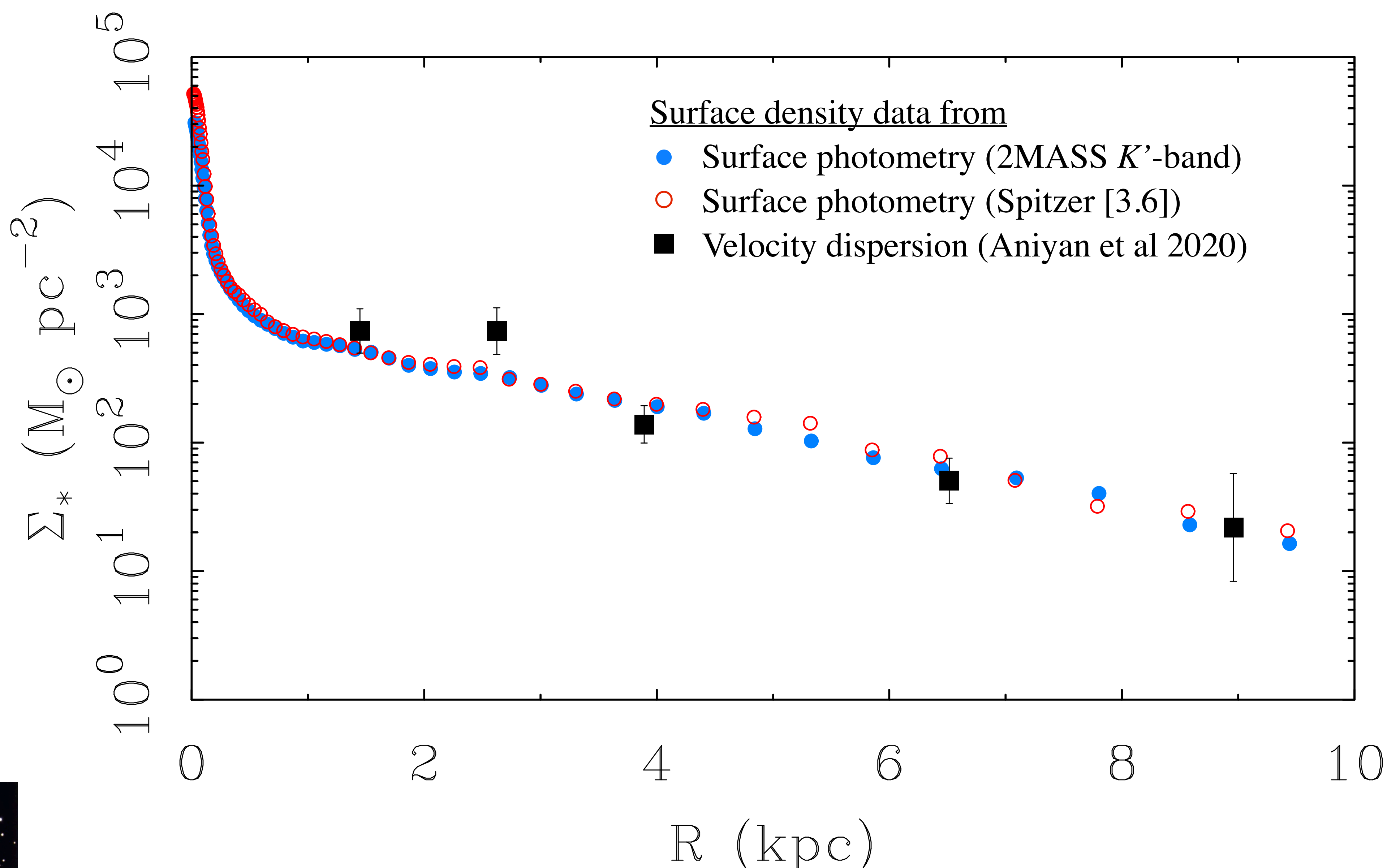

NGC 6946

Progressive approximations
in mass modeling

- Point Mass
- “spherical” disk
- thin exponential disk
- thick exponential disk
- surface density $\Sigma(R)$
- 2D $\Sigma(R, \phi)$ [e.g., bars]
- 3D $\rho(R, \phi, z)$
- 3D + non-equilibrium

We numerically solve the Poisson equation to obtain the gravitational potential Φ_* from the observed surface density $\Sigma_*(R)$

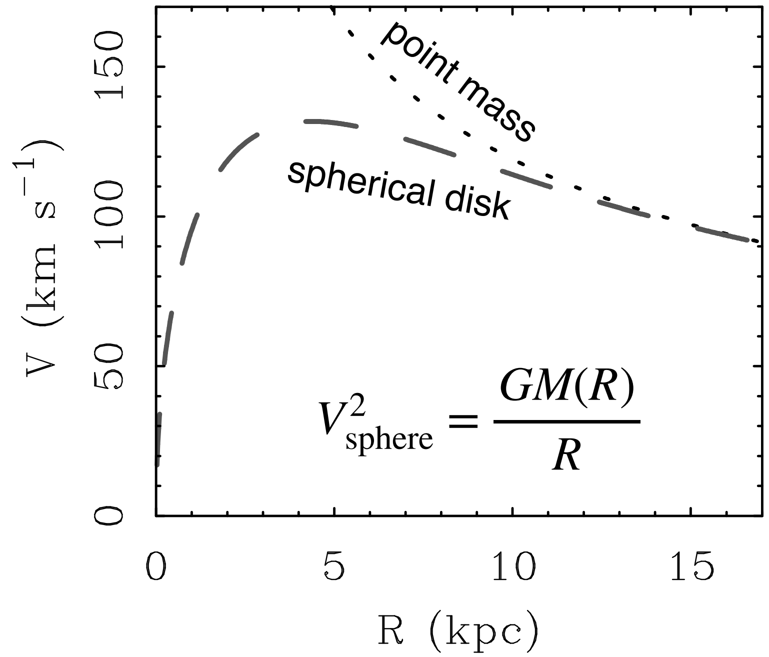

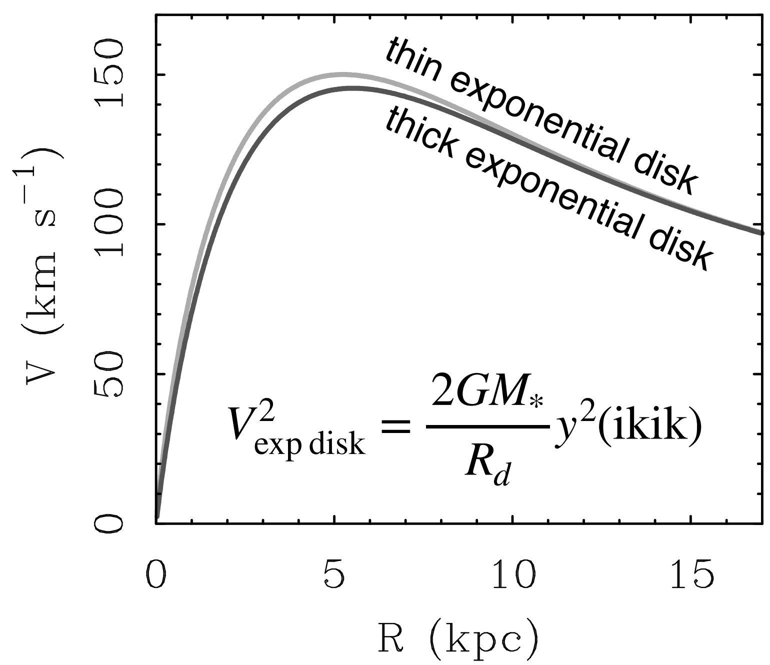

$$\mathrm{ikik} = [I_0(y)K_0(y) - I_1(y)K_1(y)]$$

$$y = \frac{R}{2R_d}$$

Examples for the size and mass of NGC 6946

$$M_* = 3.3 \times 10^{10}\ \mathrm{M}_\odot$$
$$R_d = 2.44\ \mathrm{kpc}$$

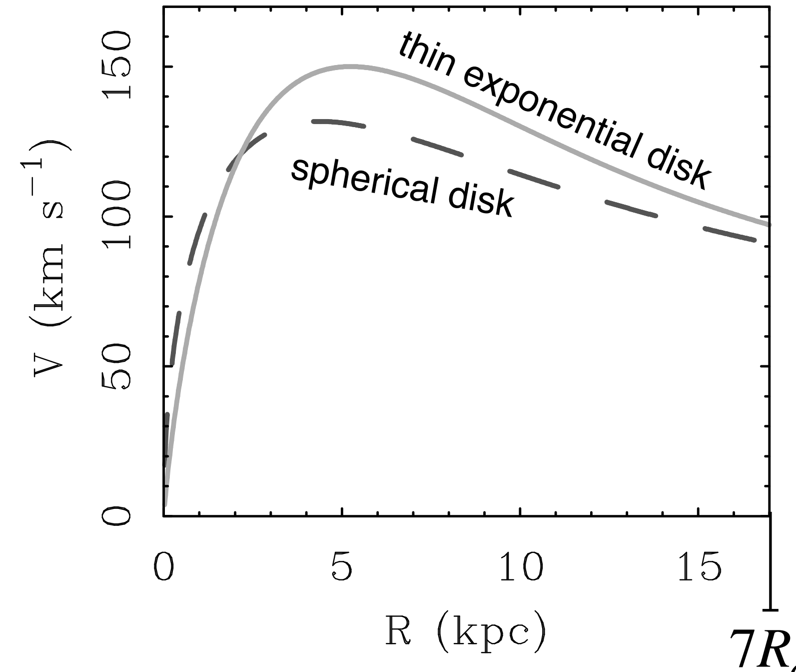

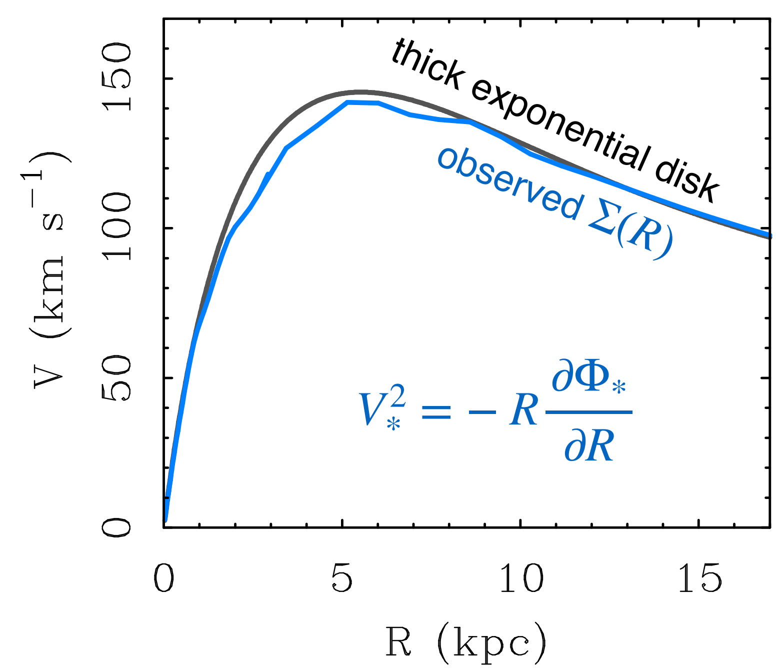

Now have

Surface density for
- stars
- gas

and corresponding rotation curves for each component

Observed rotation curve

NGC 6946

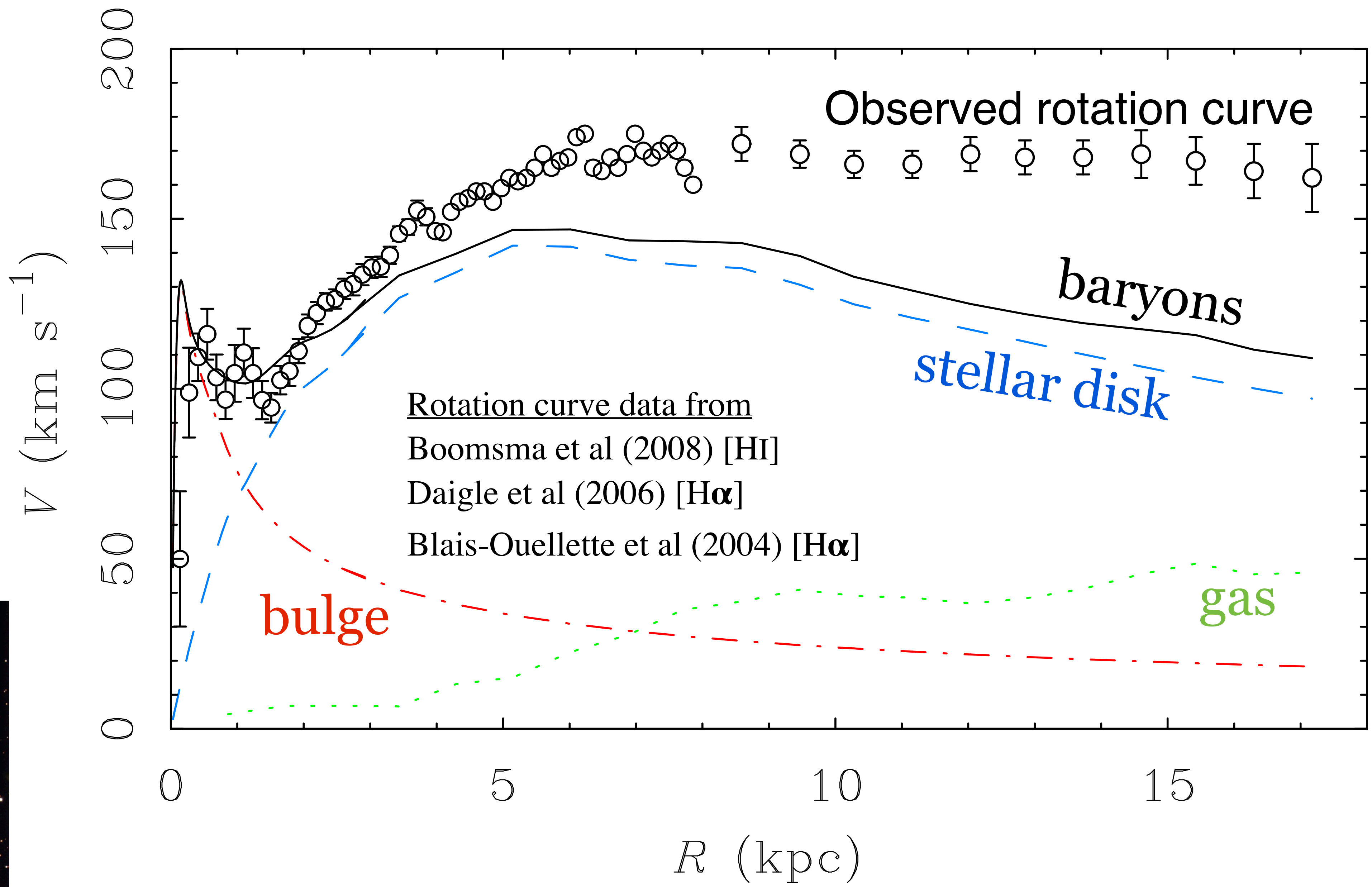

$$V^2_{\rm bar} = V^2_{\rm disk} + V^2_{\rm bulge} + V^2_{\rm gas}$$

Rotation curve shape correlates with baryonic surface density

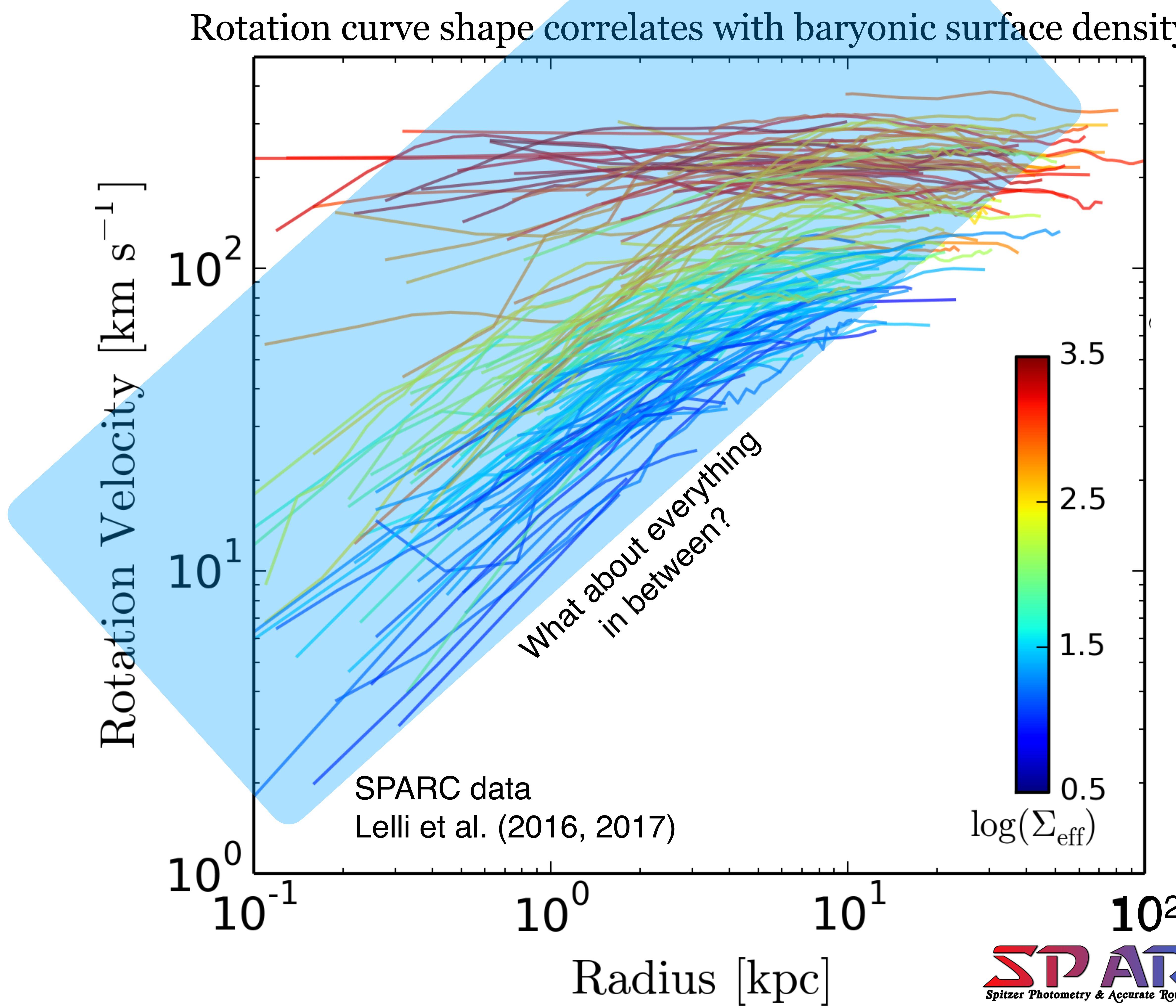

SPARC
Spitzer Photometry & Accurate Rotation Curves

What about everything in between?

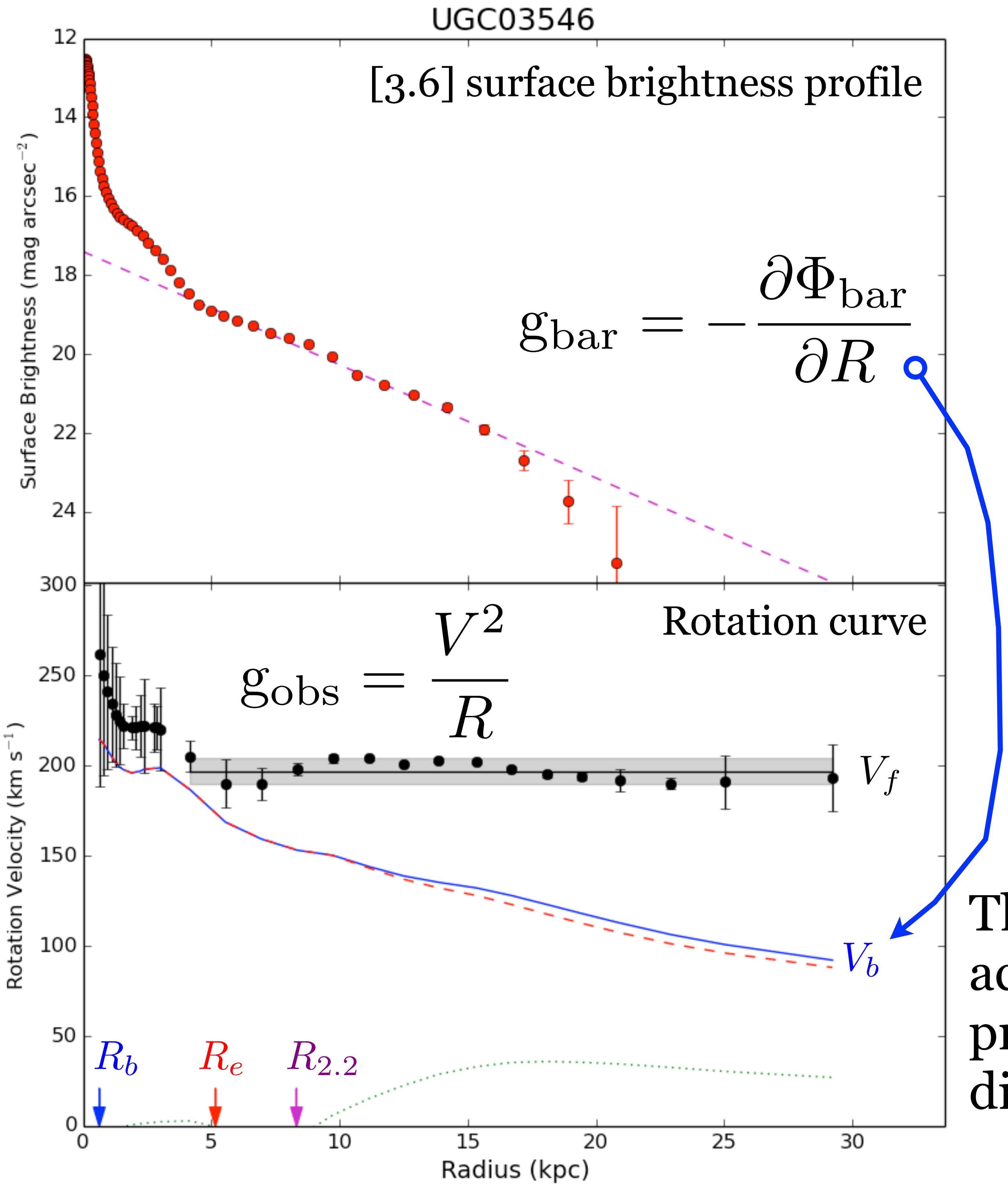

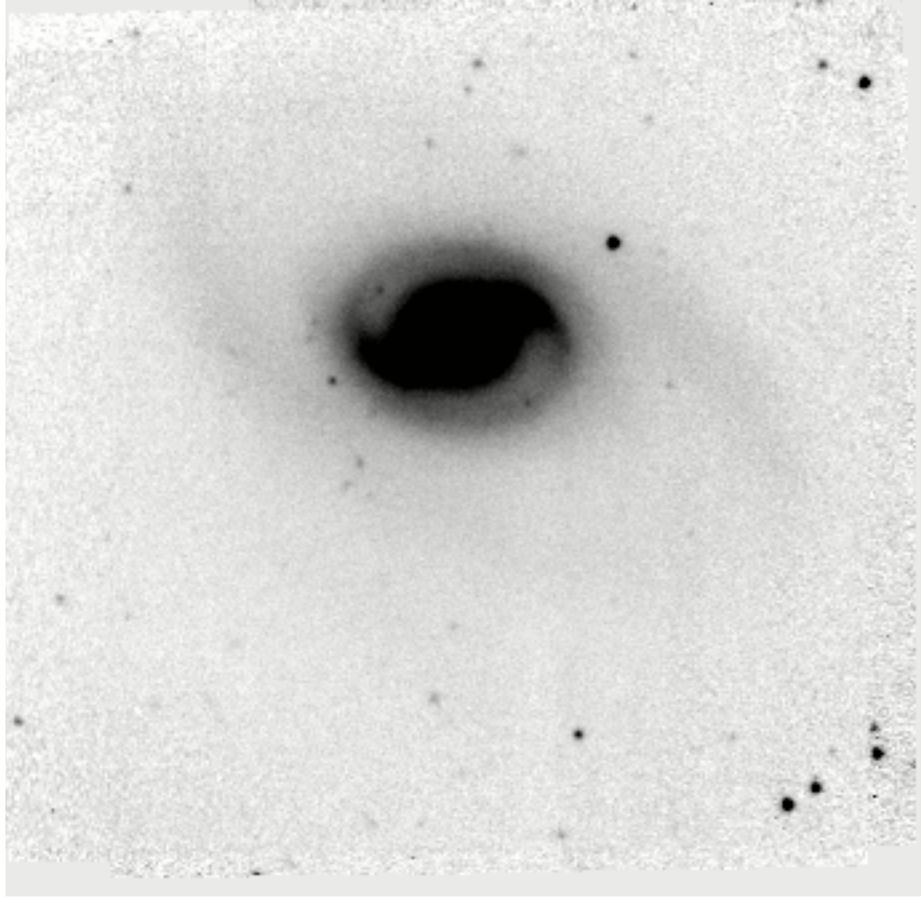

The observed centripetal acceleration is linked to that predicted by the observed distribution of baryons.

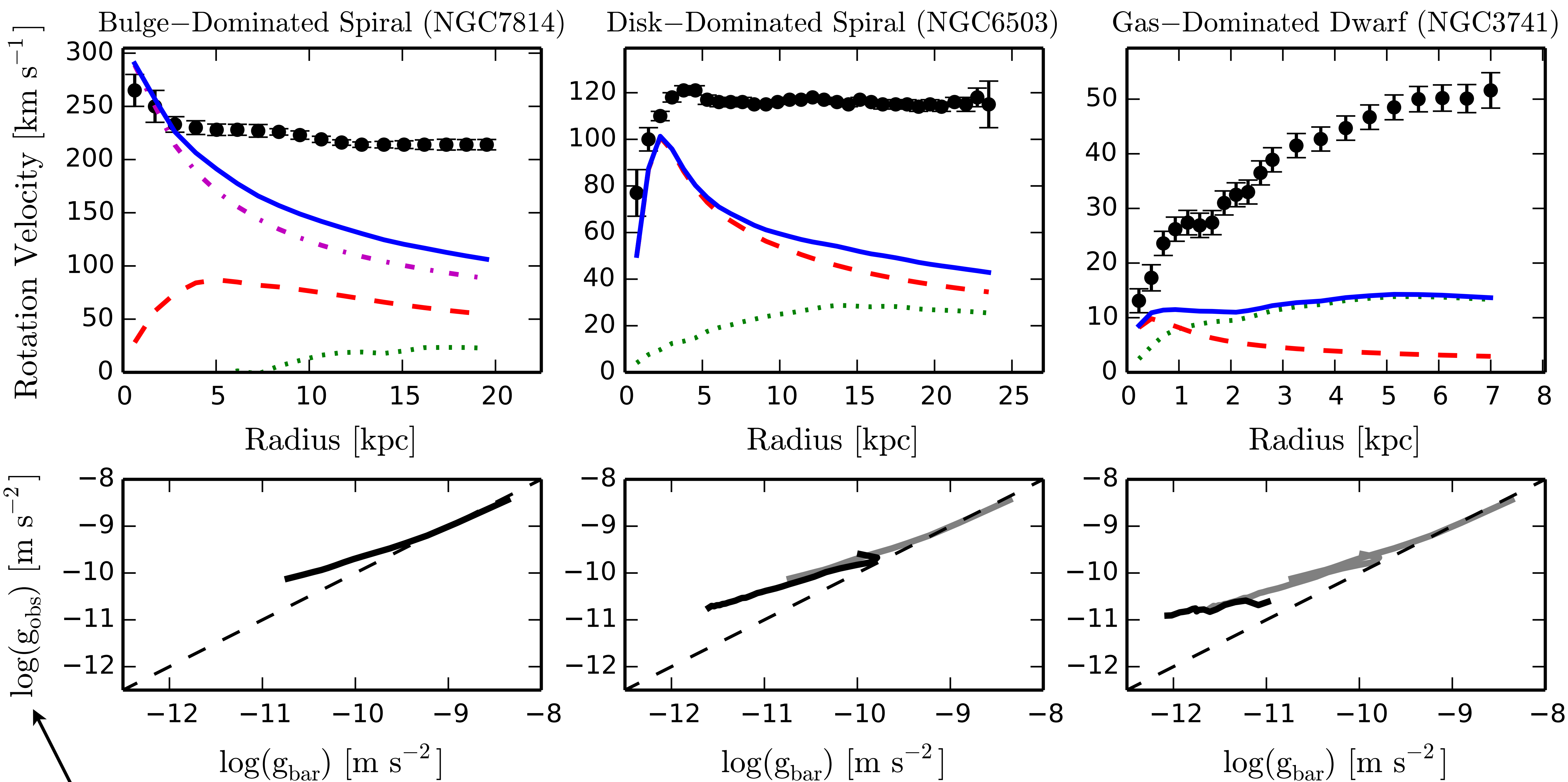

$$g_{\rm obs} = \frac{V^2}{R}$$

independent quantities

$$g_{\rm bar} = -\frac{\partial \Phi_{\rm bar}}{\partial R}$$

determined from rotation curve

determined from baryon distribution

Radial Acceleration Relation

(RAR)

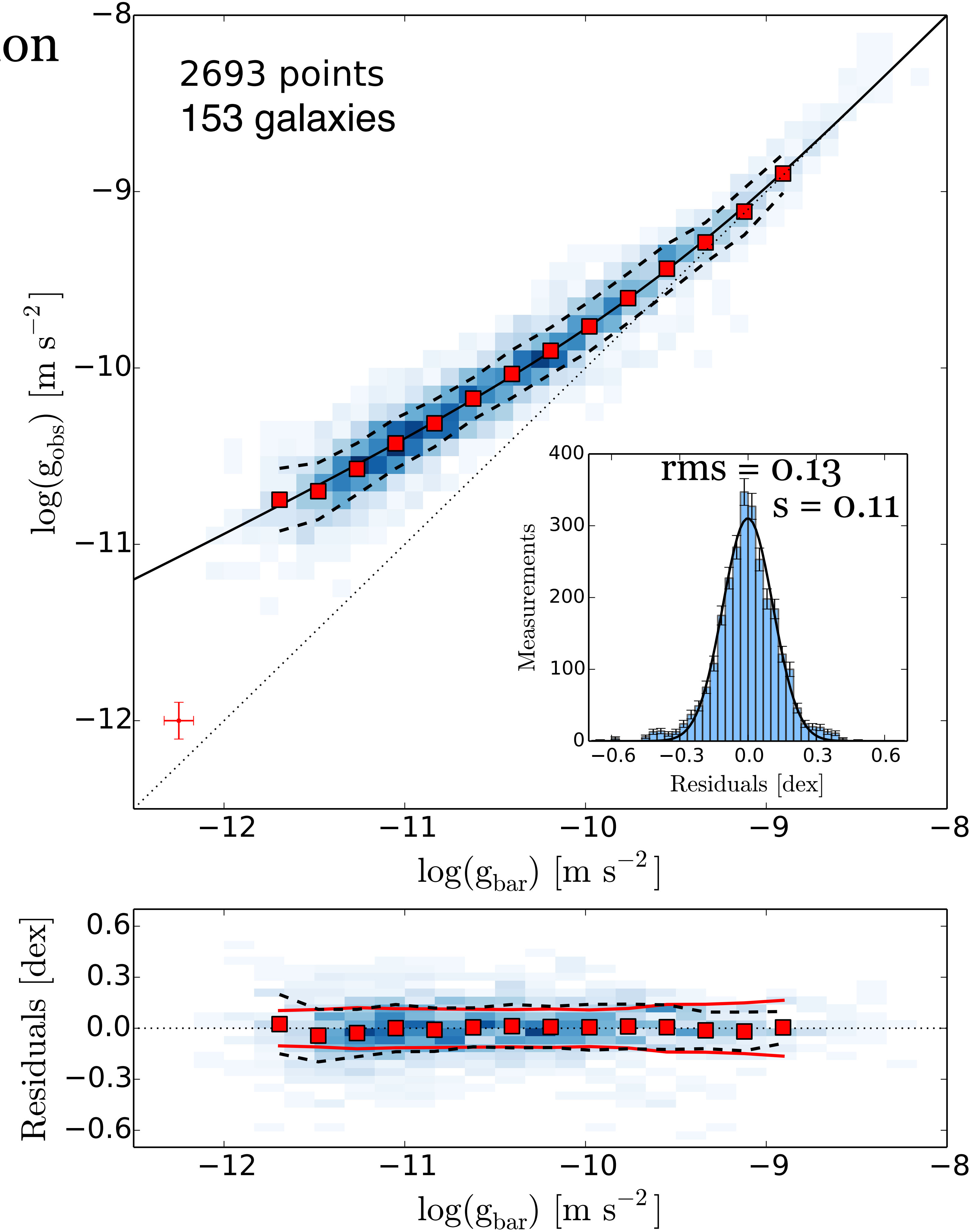

Constructed from 153 galaxies with 21cm rotation curves and near-IR surface photometry from the *Spitzer* space telescope.

Apparently the mass-to-light ratio in the near-IR is close to constant: individual galaxies do not stand out in this relation.

The Radial Acceleration Relation is equivalent to the Mass Discrepancy-acceleration relation, just with independent x & y axes.

$$\mathcal{D} = \frac{g_{obs}}{g_{bar}} = \frac{V^2}{V_b^2}$$

MDAR

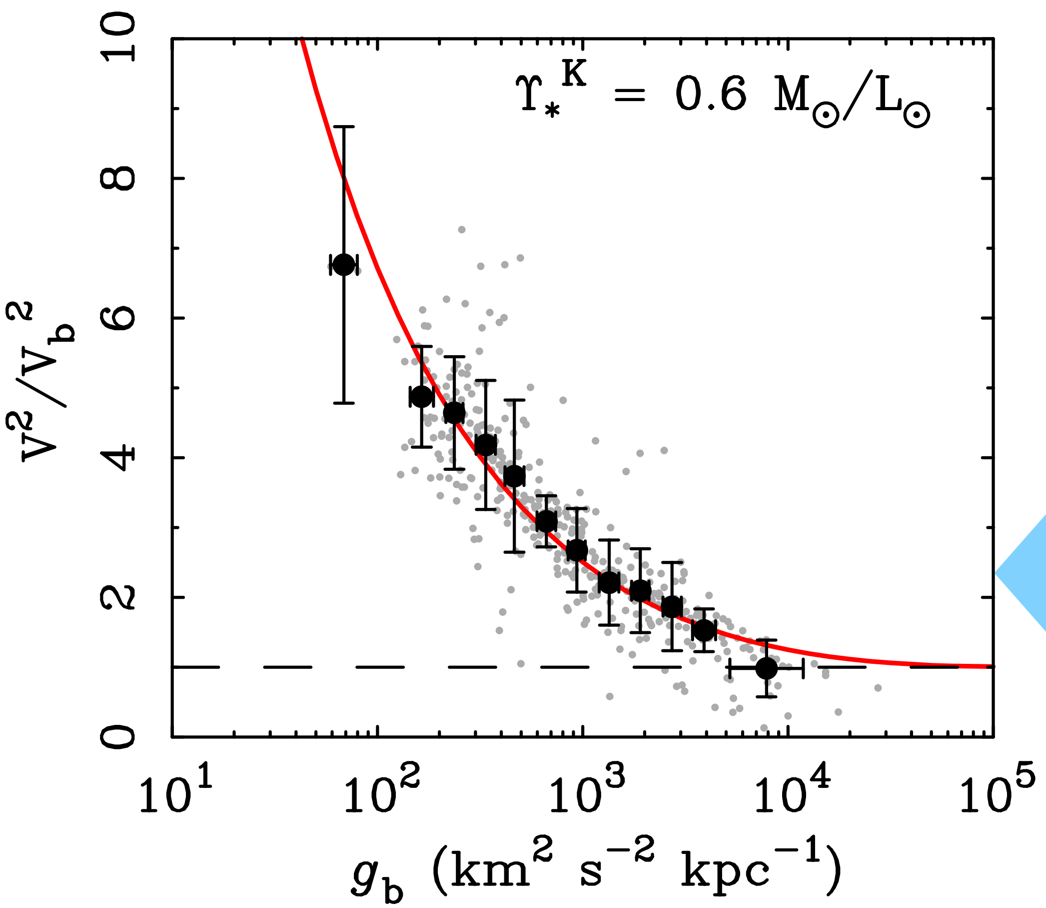

RAR

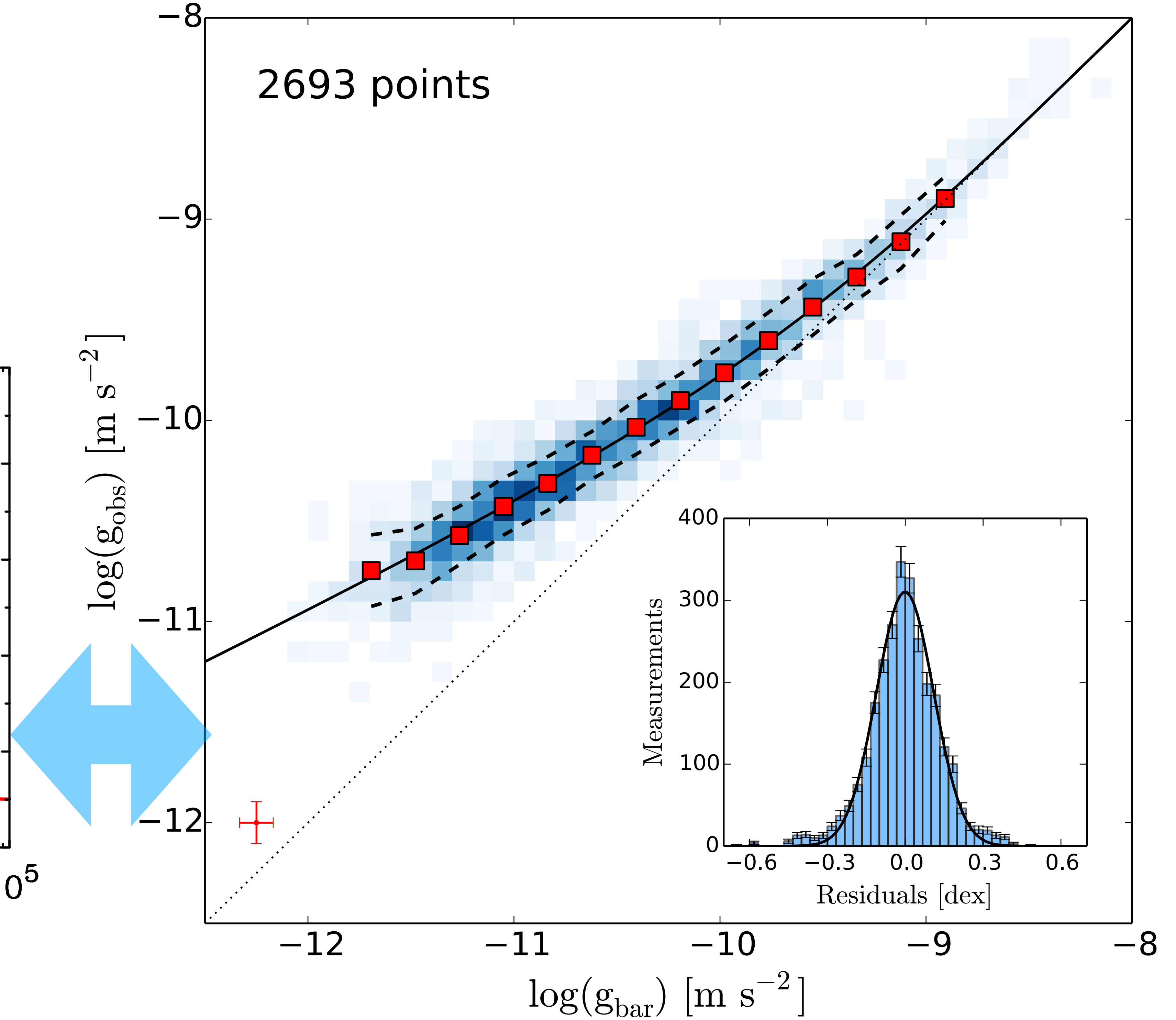

Radial Acceleration Relation

The observed acceleration correlates with that predicted by the baryons

The data are well fit by

$$g_{obs} = \frac{g_{bar}}{1 - e^{-\sqrt{g_{bar}/g_{\dagger}}}}$$

$$g_{\dagger} = 1.20 \times 10^{-10} \text{ m s}^{-2}$$

± 0.02 (random) $\pm$ 0.24 (systematic)

Lelli et al. (2017)
McGaugh et al. (2016)

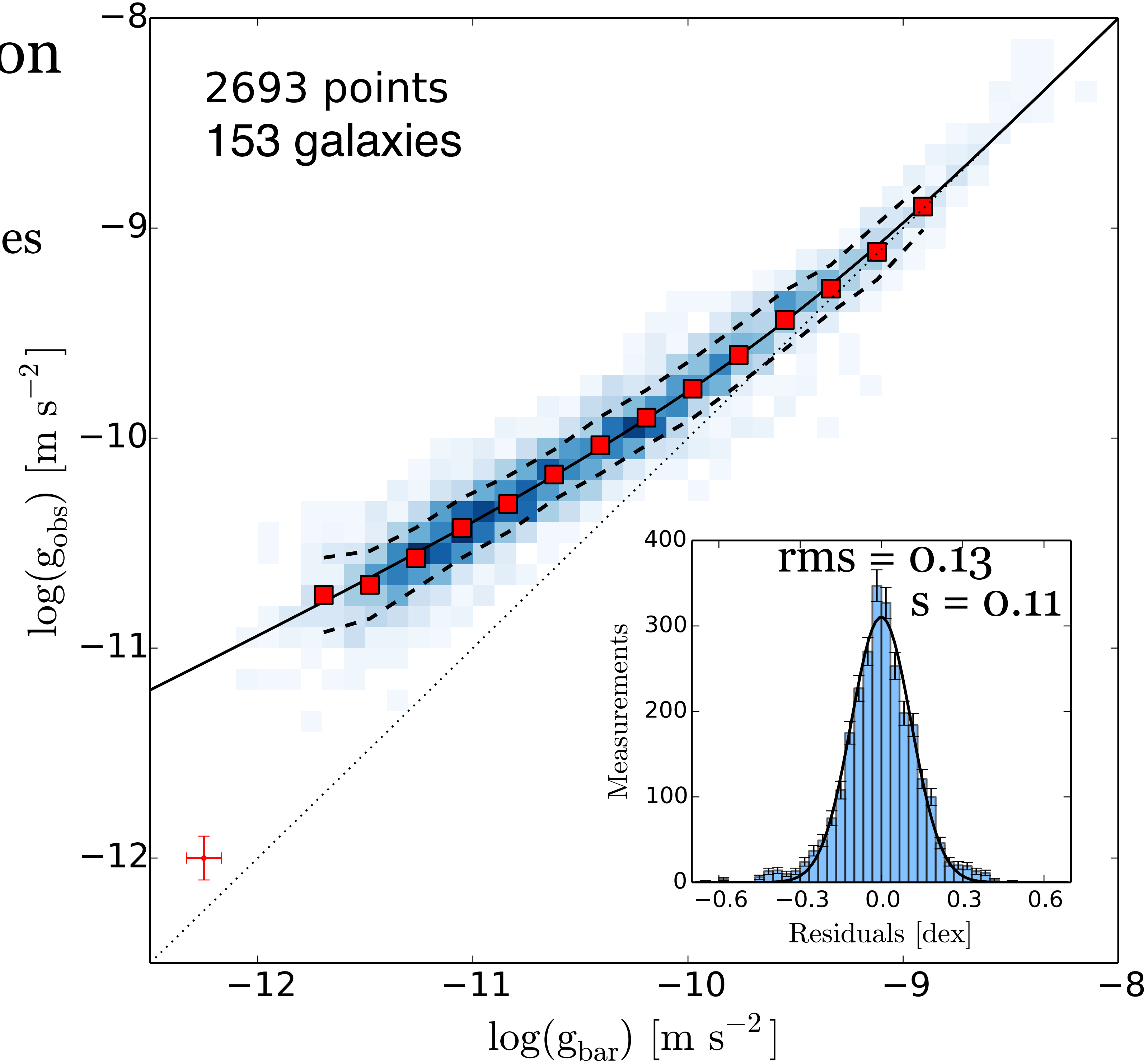

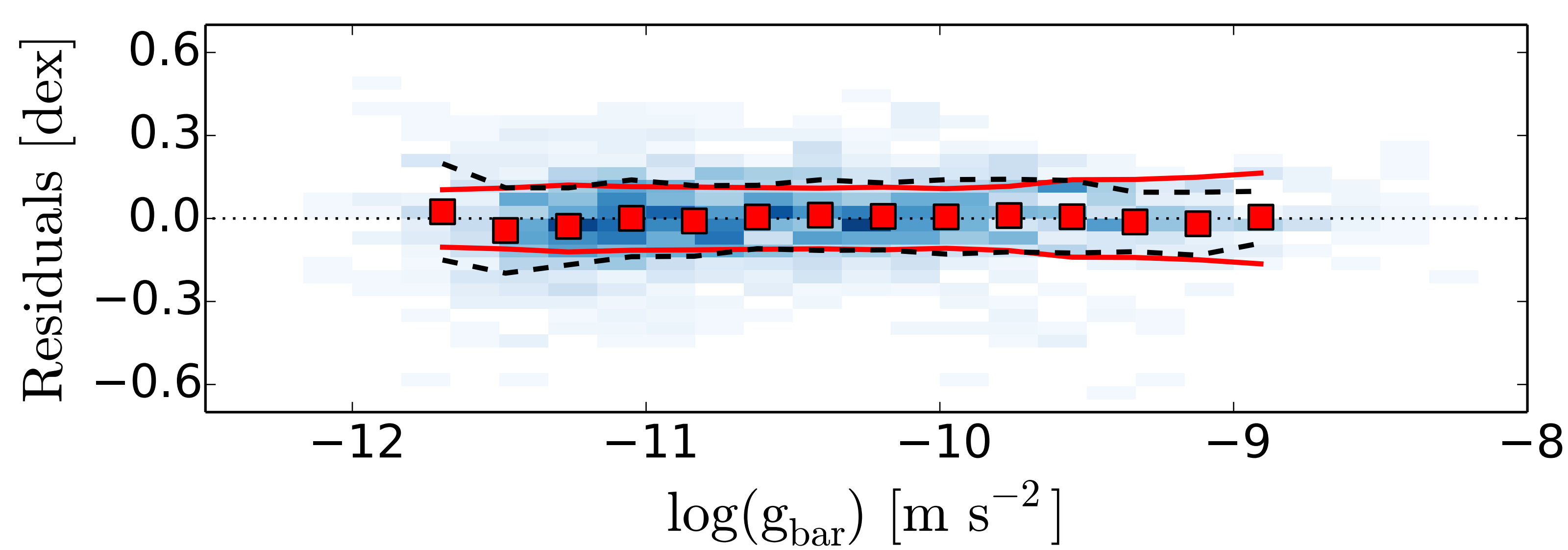

observed rms scatter

scatter expected from observational errors

The data are consistent with zero intrinsic scatter

TABLE I. Scatter Budget for Acceleration Residuals

Source	Residual
Rotation velocity errors	0.03 dex
Disk inclination errors	0.05 dex
Galaxy distance errors	0.08 dex
Variation in mass-to-light ratios	0.06 dex
HI flux calibration errors	0.01 dex
Total	0.12 dex

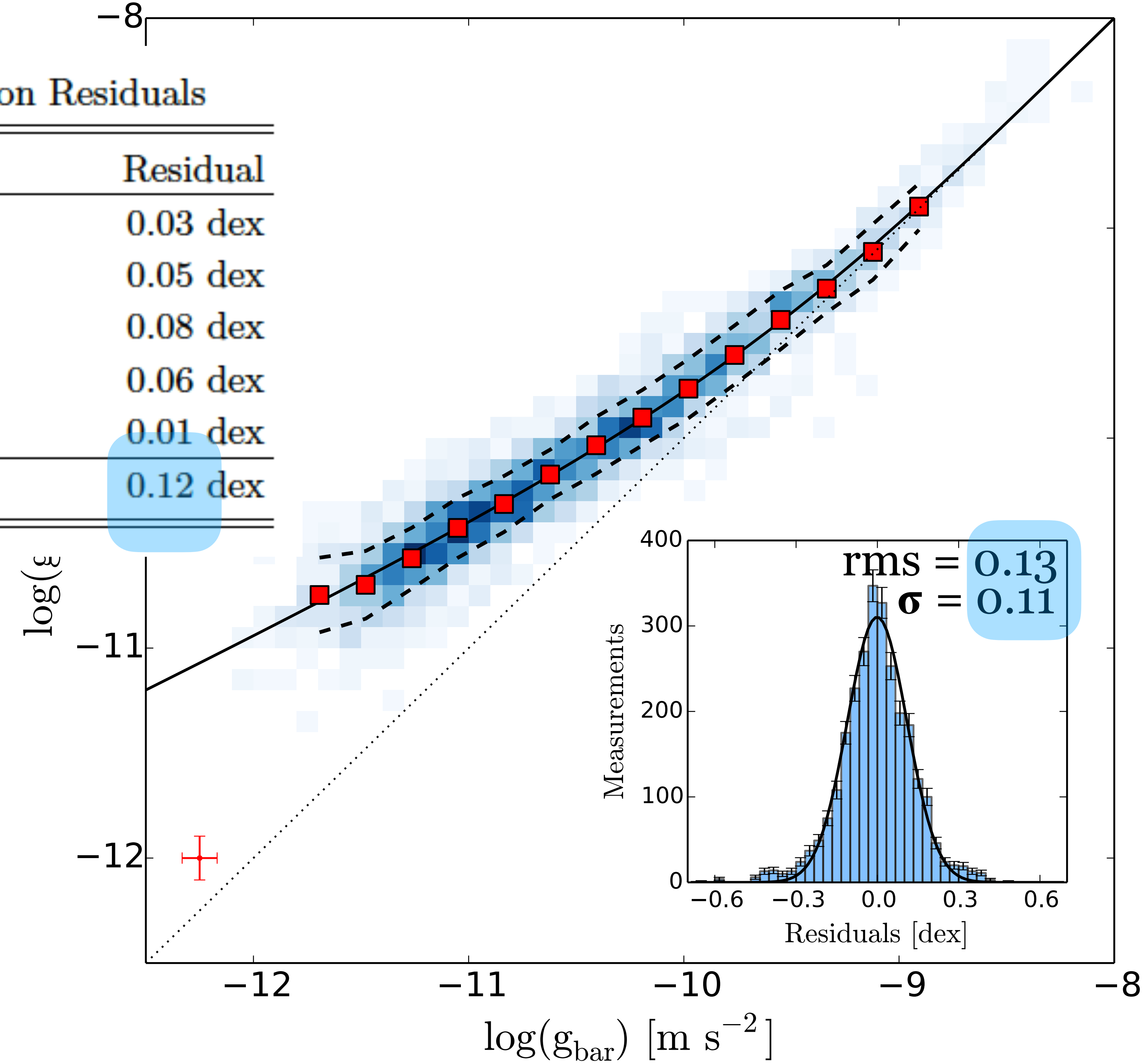

The observed scatter is consistent with that expected from known uncertainties: the radial acceleration relation is consistent has negligible intrinsic scatter.

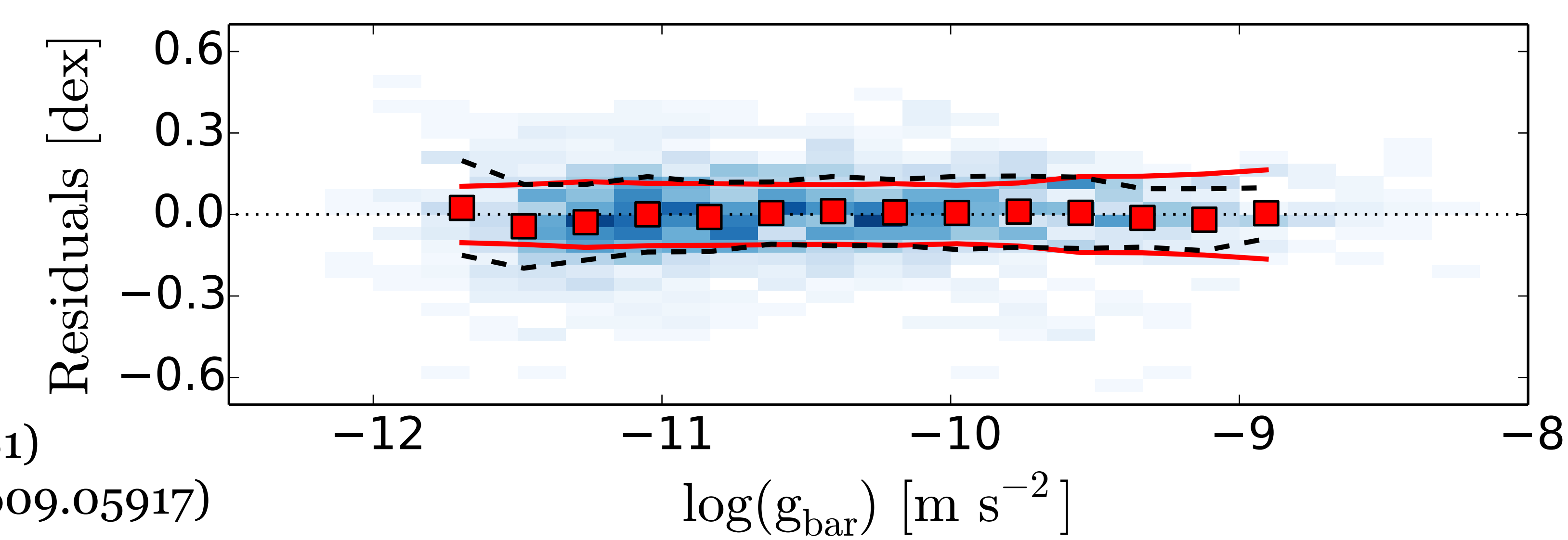

Lelli et al. 2017, ApJ, 836, 152 (arXiv:1610.08981)
McGaugh et al. 2016, PRL, 117, 201101 (arXiv:1609.05917)

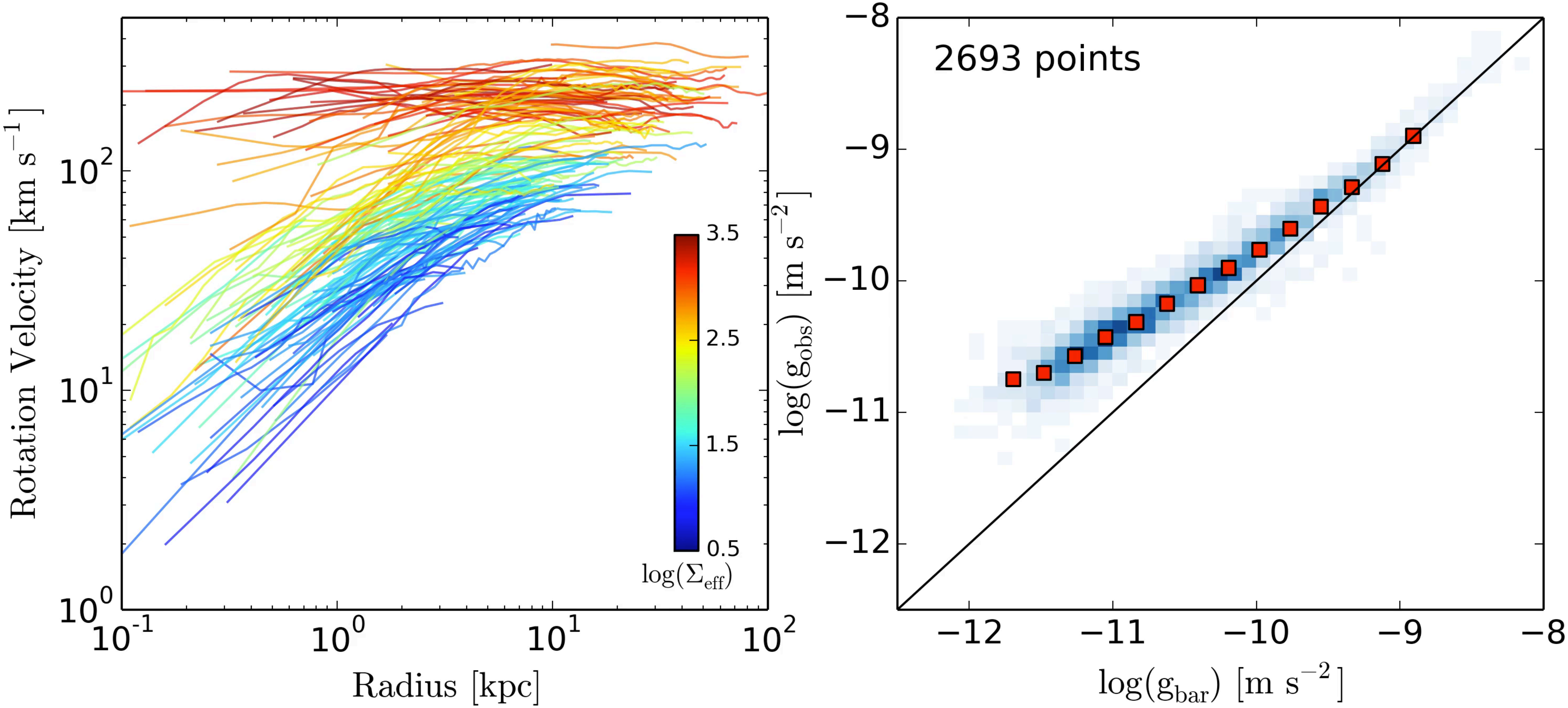

http://astroweb.case.edu/SPARC/RARmovie.mp4

That just assumed constant M*/L. We can fit to the mean RAR, marginalizing over distance and inclination as nuisance parameters (Li et al. 2018)

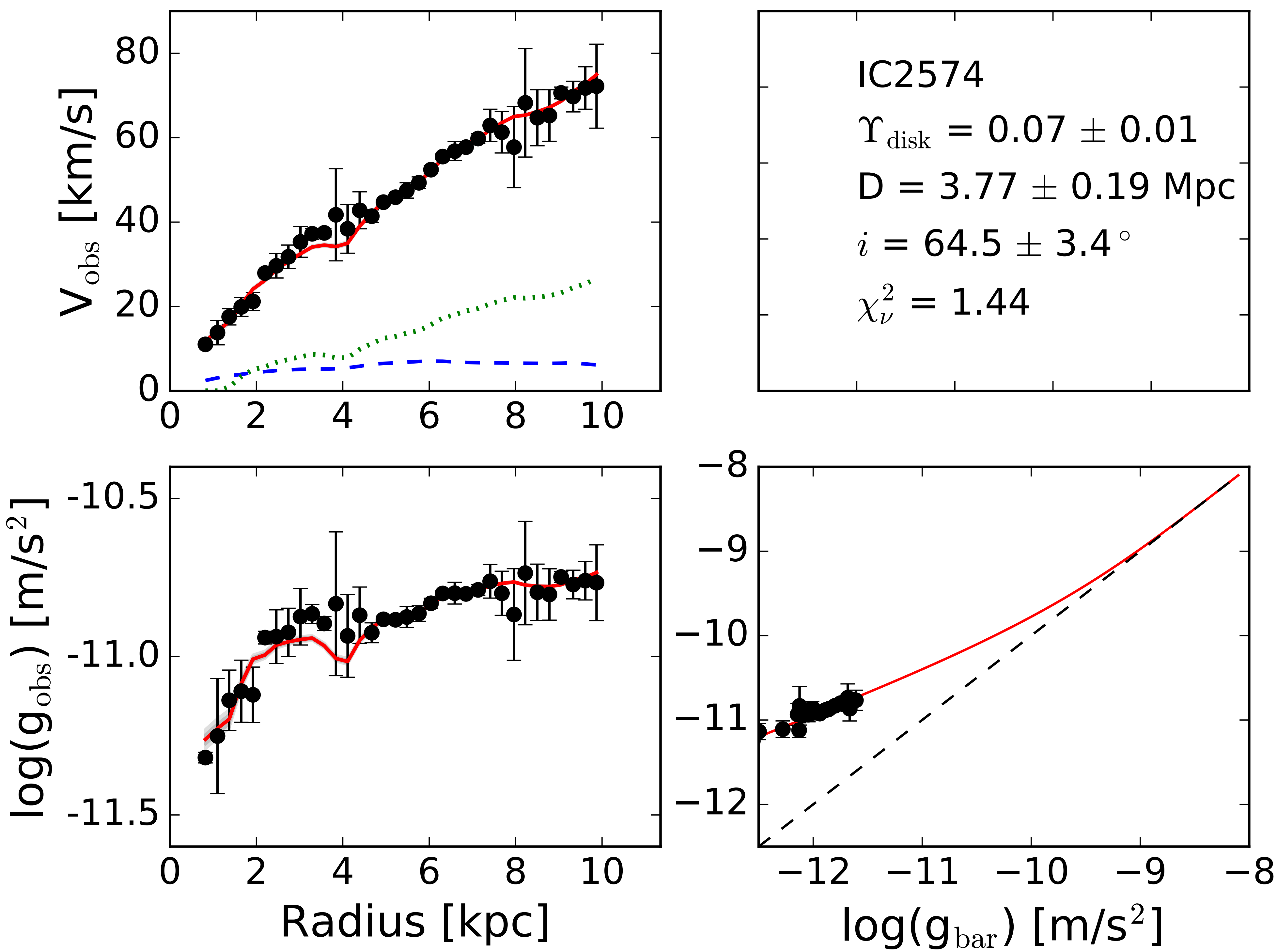

Li et al. 2018, A&A, 615, A3 (arXiv:1803.00022)

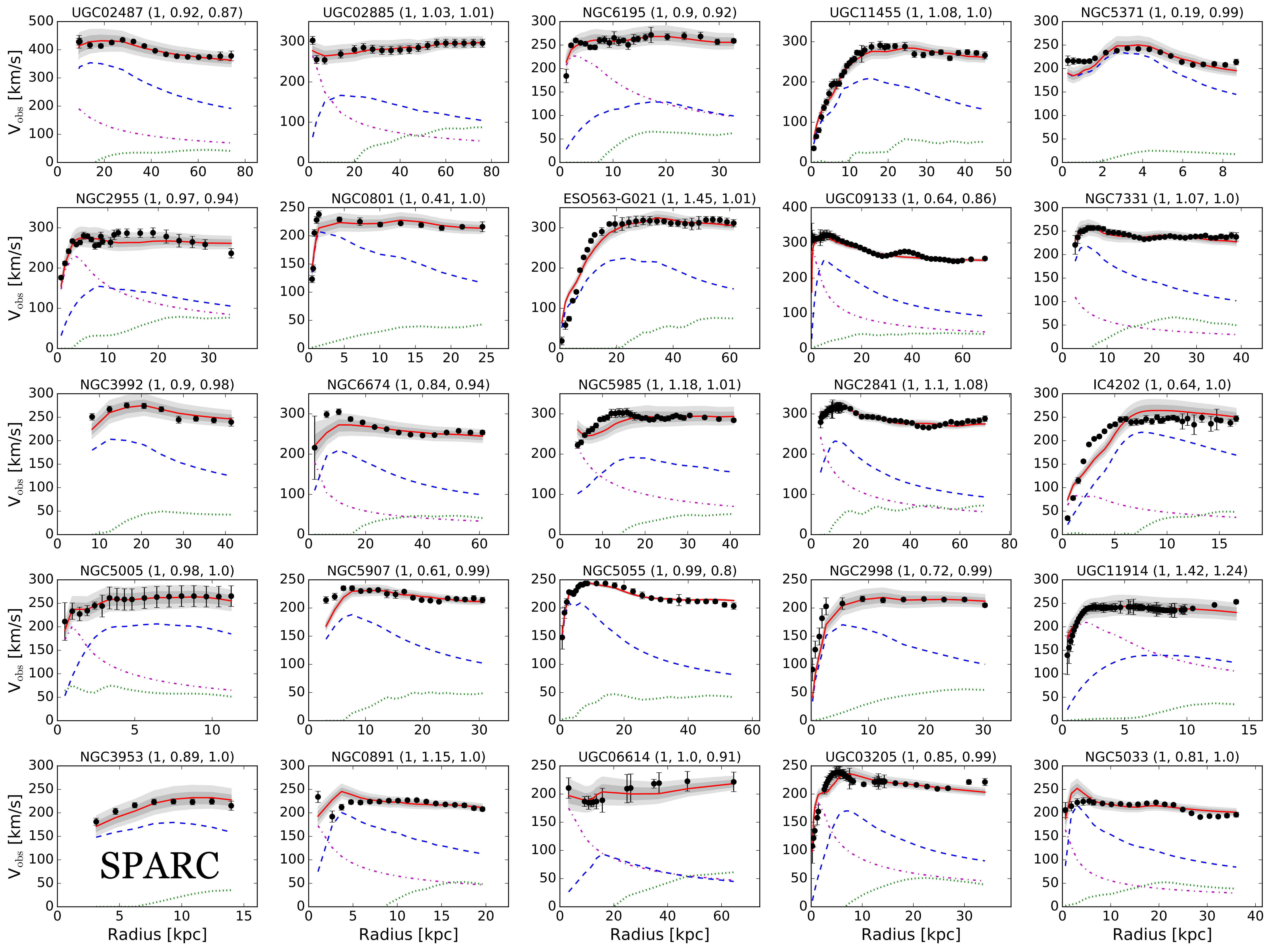
UGC02487 (1, 0.92, 0.87)
UGC02885 (1, 1.03, 1.01)
NGC6195 (1, 0.9, 0.92)
UGC11455 (1, 1.08, 1.0)
NGC5371 (1, 0.19, 0.99)
NGC2955 (1, 0.97, 0.94)
NGC0801 (1, 0.41, 1.0)
ESO563-G021 (1, 1.45, 1.01)
UGC09133 (1, 0.64, 0.86)
NGC7331 (1, 1.07, 1.0)
NGC3992 (1, 0.9, 0.98)
NGC6674 (1, 0.84, 0.94)
NGC5985 (1, 1.18, 1.01)
NGC2841 (1, 1.1, 1.08)
IC4202 (1, 0.64, 1.0)
NGC5005 (1, 0.98, 1.0)
NGC5907 (1, 0.61, 0.99)
NGC5055 (1, 0.99, 0.8)
NGC2998 (1, 0.72, 0.99)
UGC11914 (1, 1.42, 1.24)
NGC3953 (1, 0.89, 1.0)
NGC0891 (1, 1.15, 1.0)
UGC06614 (1, 1.0, 0.91)
UGC03205 (1, 0.85, 0.99)
NGC5033 (1, 0.81, 1.0)
V_{obs} [km/s]
Radius [kpc]
SPARC

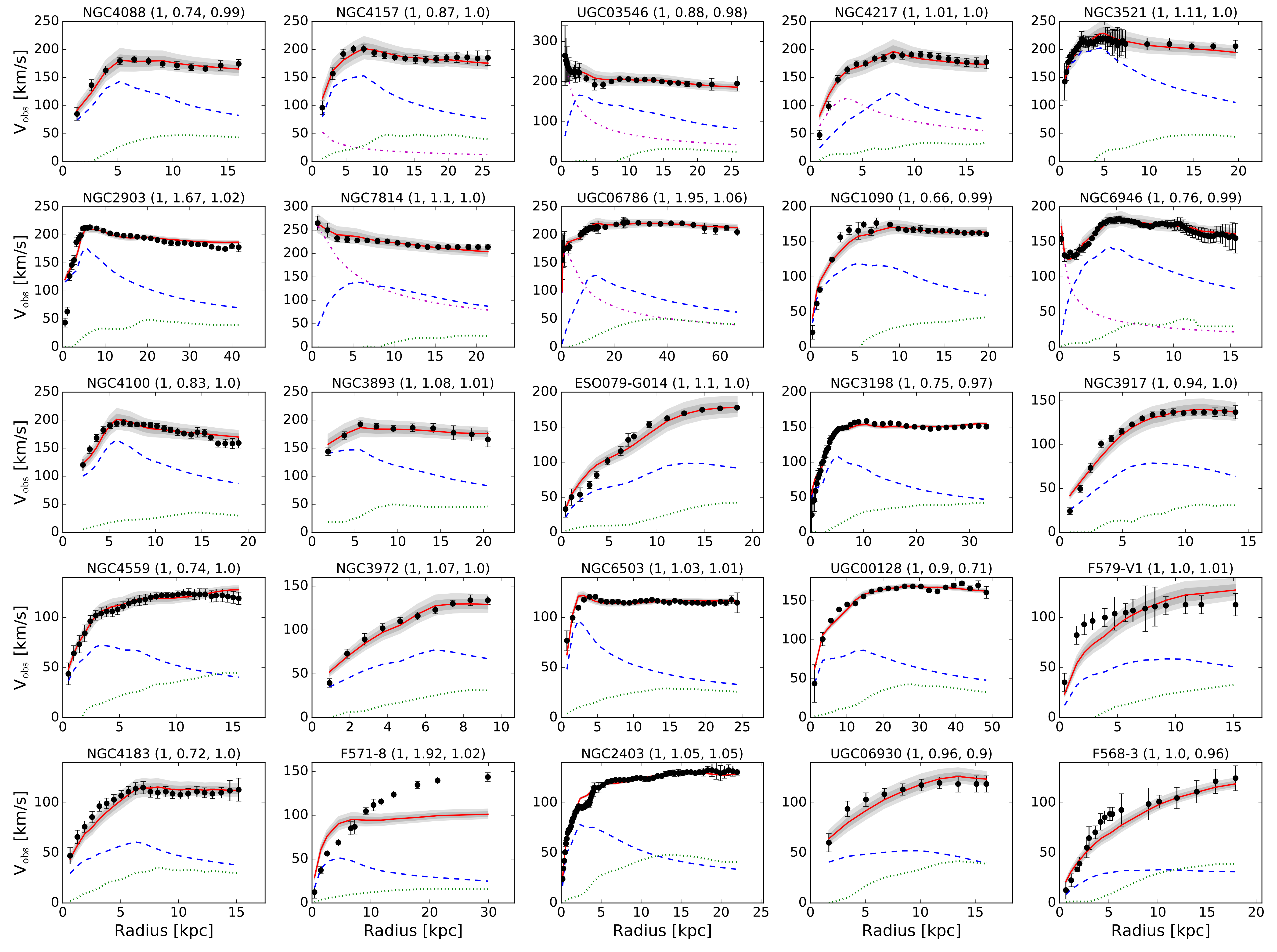
NGC4088 (1, 0.74, 0.99)
NGC4157 (1, 0.87, 1.0)
UGC03546 (1, 0.88, 0.98)
NGC4217 (1, 1.01, 1.0)
NGC3521 (1, 1.11, 1.0)
NGC2903 (1, 1.67, 1.02)
NGC7814 (1, 1.1, 1.0)
UGC06786 (1, 1.95, 1.06)
NGC1090 (1, 0.66, 0.99)
NGC6946 (1, 0.76, 0.99)
NGC4100 (1, 0.83, 1.0)
NGC3893 (1, 1.08, 1.01)
ESO079-G014 (1, 1.1, 1.0)
NGC3198 (1, 0.75, 0.97)
NGC3917 (1, 0.94, 1.0)
NGC4559 (1, 0.74, 1.0)
NGC3972 (1, 1.07, 1.0)
NGC6503 (1, 1.03, 1.01)
UGC00128 (1, 0.9, 0.71)
F579-V1 (1, 1.0, 1.01)
NGC4183 (1, 0.72, 1.0)
F571-8 (1, 1.92, 1.02)
NGC2403 (1, 1.05, 1.05)
UGC06930 (1, 0.96, 0.9)
F568-3 (1, 1.0, 0.96)
V_{obs} [km/s]
Radius [kpc]

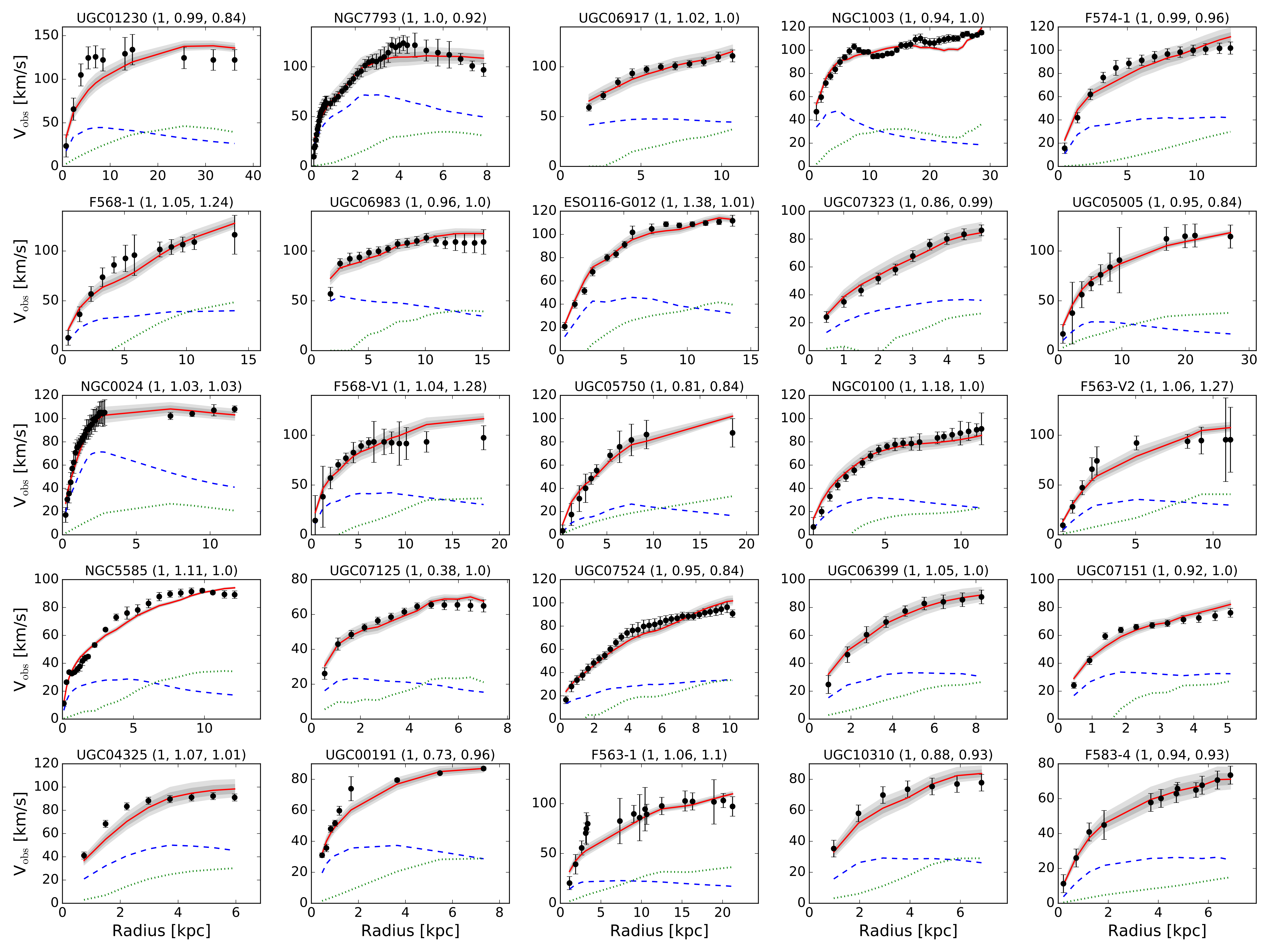
UGC01230 (1, 0.99, 0.84)
NGC7793 (1, 1.0, 0.92)
UGC06917 (1, 1.02, 1.0)
NGC1003 (1, 0.94, 1.0)
F574-1 (1, 0.99, 0.96)
F568-1 (1, 1.05, 1.24)
UGC06983 (1, 0.96, 1.0)
ESO116-G012 (1, 1.38, 1.01)
UGC07323 (1, 0.86, 0.99)
UGC05005 (1, 0.95, 0.84)
NGC0024 (1, 1.03, 1.03)
F568-V1 (1, 1.04, 1.28)
UGC05750 (1, 0.81, 0.84)
NGC0100 (1, 1.18, 1.0)
F563-V2 (1, 1.06, 1.27)
NGC5585 (1, 1.11, 1.0)
UGC07125 (1, 0.38, 1.0)
UGC07524 (1, 0.95, 0.84)
UGC06399 (1, 1.05, 1.0)
UGC07151 (1, 0.92, 1.0)
UGC04325 (1, 1.07, 1.01)
UGC00191 (1, 0.73, 0.96)
F563-1 (1, 1.06, 1.1)
UGC10310 (1, 0.88, 0.93)
F583-4 (1, 0.94, 0.93)
V_{obs} [km/s]
Radius [kpc]

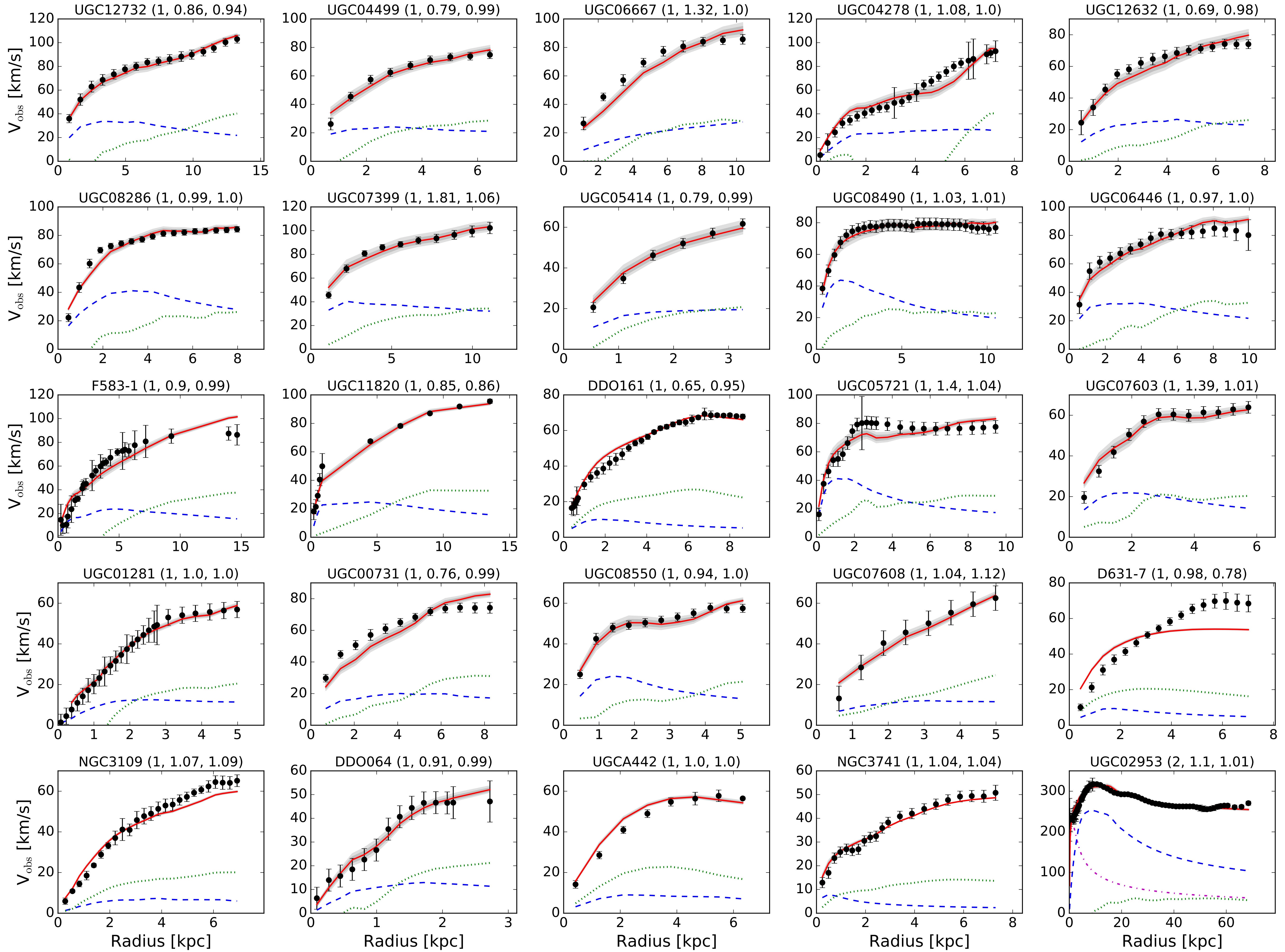
UGC12732 (1, 0.86, 0.94)
UGC04499 (1, 0.79, 0.99)
UGC06667 (1, 1.32, 1.0)
UGC04278 (1, 1.08, 1.0)
UGC12632 (1, 0.69, 0.98)
UGC08286 (1, 0.99, 1.0)
UGC07399 (1, 1.81, 1.06)
UGC05414 (1, 0.79, 0.99)
UGC08490 (1, 1.03, 1.01)
UGC06446 (1, 0.97, 1.0)
F583-1 (1, 0.9, 0.99)
UGC11820 (1, 0.85, 0.86)
DDO161 (1, 0.65, 0.95)
UGC05721 (1, 1.4, 1.04)
UGC07603 (1, 1.39, 1.01)
UGC01281 (1, 1.0, 1.0)
UGC00731 (1, 0.76, 0.99)
UGC08550 (1, 0.94, 1.0)
UGC07608 (1, 1.04, 1.12)
D631-7 (1, 0.98, 0.78)
NGC3109 (1, 1.07, 1.09)
DDO064 (1, 0.91, 0.99)
UGCA442 (1, 1.0, 1.0)
NGC3741 (1, 1.04, 1.04)
UGC02953 (2, 1.1, 1.01)
V_{obs} [km/s]
Radius [kpc]

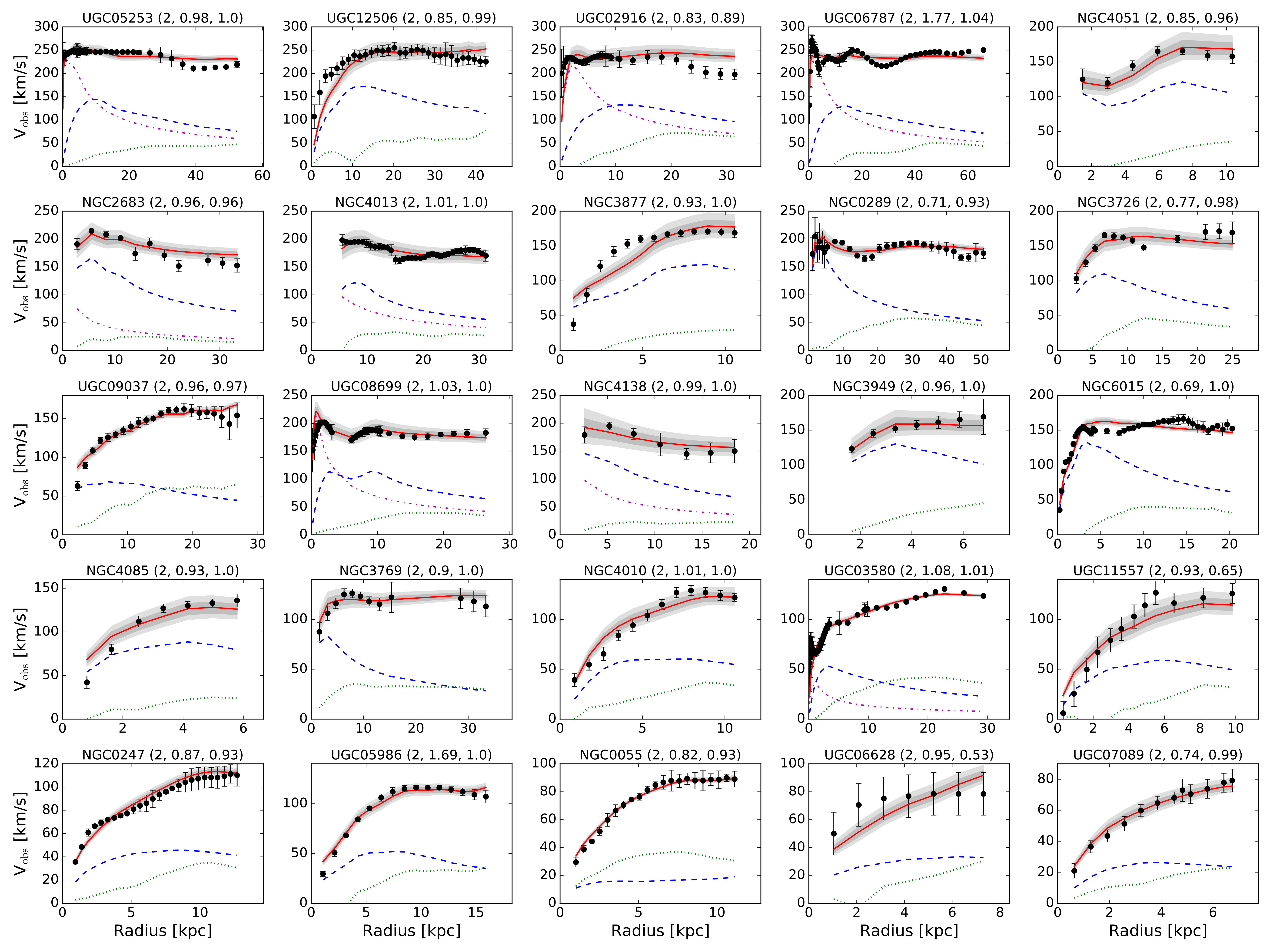
UGC05253 (2, 0.98, 1.0)
UGC12506 (2, 0.85, 0.99)
UGC02916 (2, 0.83, 0.89)
UGC06787 (2, 1.77, 1.04)
NGC4051 (2, 0.85, 0.96)
NGC2683 (2, 0.96, 0.96)
NGC4013 (2, 1.01, 1.0)
NGC3877 (2, 0.93, 1.0)
NGC0289 (2, 0.71, 0.93)
NGC3726 (2, 0.77, 0.98)
UGC09037 (2, 0.96, 0.97)
UGC08699 (2, 1.03, 1.0)
NGC4138 (2, 0.99, 1.0)
NGC3949 (2, 0.96, 1.0)
NGC6015 (2, 0.69, 1.0)
NGC4085 (2, 0.93, 1.0)
NGC3769 (2, 0.9, 1.0)
NGC4010 (2, 1.01, 1.0)
UGC03580 (2, 1.08, 1.01)
UGC11557 (2, 0.93, 0.65)
NGC0247 (2, 0.87, 0.93)
UGC05986 (2, 1.69, 1.0)
NGC0055 (2, 0.82, 0.93)
UGC06628 (2, 0.95, 0.53)
UGC07089 (2, 0.74, 0.99)
V_obs [km/s]
Radius [kpc]

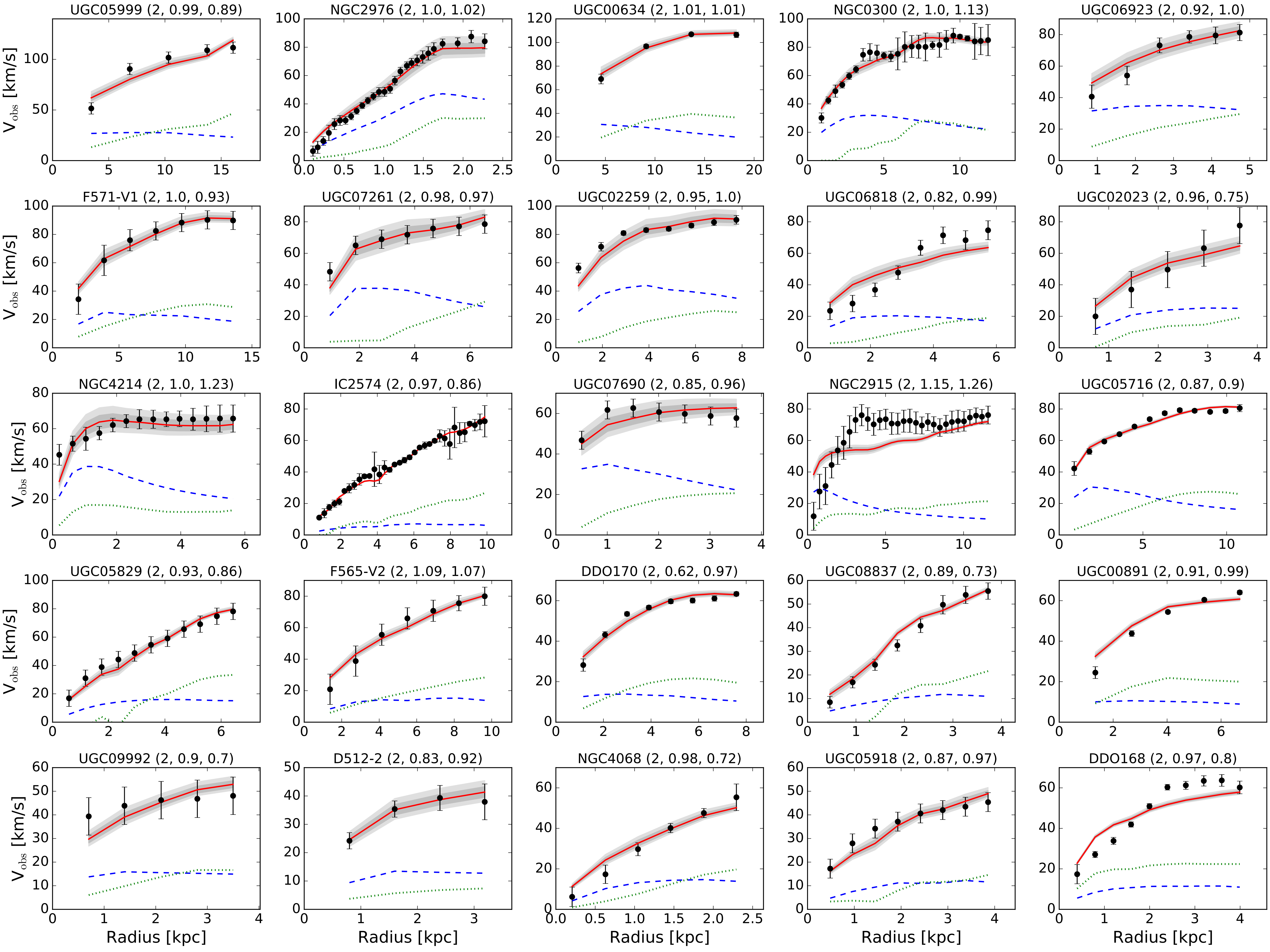
UGC05999 (2, 0.99, 0.89)
NGC2976 (2, 1.0, 1.02)
UGC00634 (2, 1.01, 1.01)
NGC0300 (2, 1.0, 1.13)
UGC06923 (2, 0.92, 1.0)
F571-V1 (2, 1.0, 0.93)
UGC07261 (2, 0.98, 0.97)
UGC02259 (2, 0.95, 1.0)
UGC06818 (2, 0.82, 0.99)
UGC02023 (2, 0.96, 0.75)
NGC4214 (2, 1.0, 1.23)
IC2574 (2, 0.97, 0.86)
UGC07690 (2, 0.85, 0.96)
NGC2915 (2, 1.15, 1.26)
UGC05716 (2, 0.87, 0.9)
UGC05829 (2, 0.93, 0.86)
F565-V2 (2, 1.09, 1.07)
DDO170 (2, 0.62, 0.97)
UGC08837 (2, 0.89, 0.73)
UGC00891 (2, 0.91, 0.99)
UGC09992 (2, 0.9, 0.7)
D512-2 (2, 0.83, 0.92)
NGC4068 (2, 0.98, 0.72)
UGC05918 (2, 0.87, 0.97)
DDO168 (2, 0.97, 0.8)
V_{obs} [km/s]
Radius [kpc]

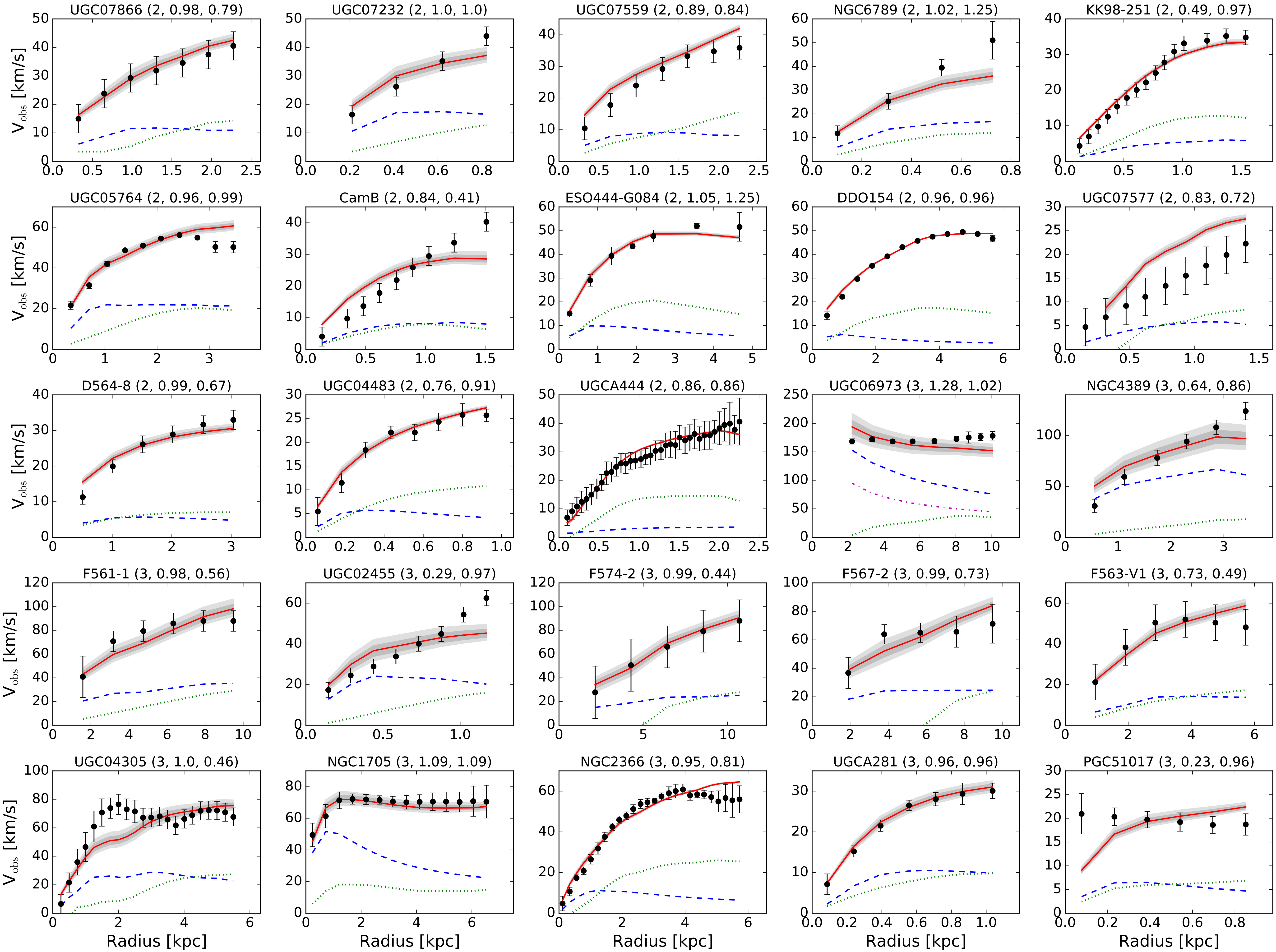
UGC07866 (2, 0.98, 0.79)
UGC07232 (2, 1.0, 1.0)
UGC07559 (2, 0.89, 0.84)
NGC6789 (2, 1.02, 1.25)
KK98-251 (2, 0.49, 0.97)
UGC05764 (2, 0.96, 0.99)
CamB (2, 0.84, 0.41)
ESO444-G084 (2, 1.05, 1.25)
DDO154 (2, 0.96, 0.96)
UGC07577 (2, 0.83, 0.72)
D564-8 (2, 0.99, 0.67)
UGC04483 (2, 0.76, 0.91)
UGCA444 (2, 0.86, 0.86)
UGC06973 (3, 1.28, 1.02)
NGC4389 (3, 0.64, 0.86)
F561-1 (3, 0.98, 0.56)
UGC02455 (3, 0.29, 0.97)
F574-2 (3, 0.99, 0.44)
F567-2 (3, 0.99, 0.73)
F563-V1 (3, 0.73, 0.49)
UGC04305 (3, 1.0, 0.46)
NGC1705 (3, 1.09, 1.09)
NGC2366 (3, 0.95, 0.81)
UGCA281 (3, 0.96, 0.96)
PGC51017 (3, 0.23, 0.96)
V_{obs} [km/s]
Radius [kpc]

Residuals from SPARC data
(Li et al. 2018)

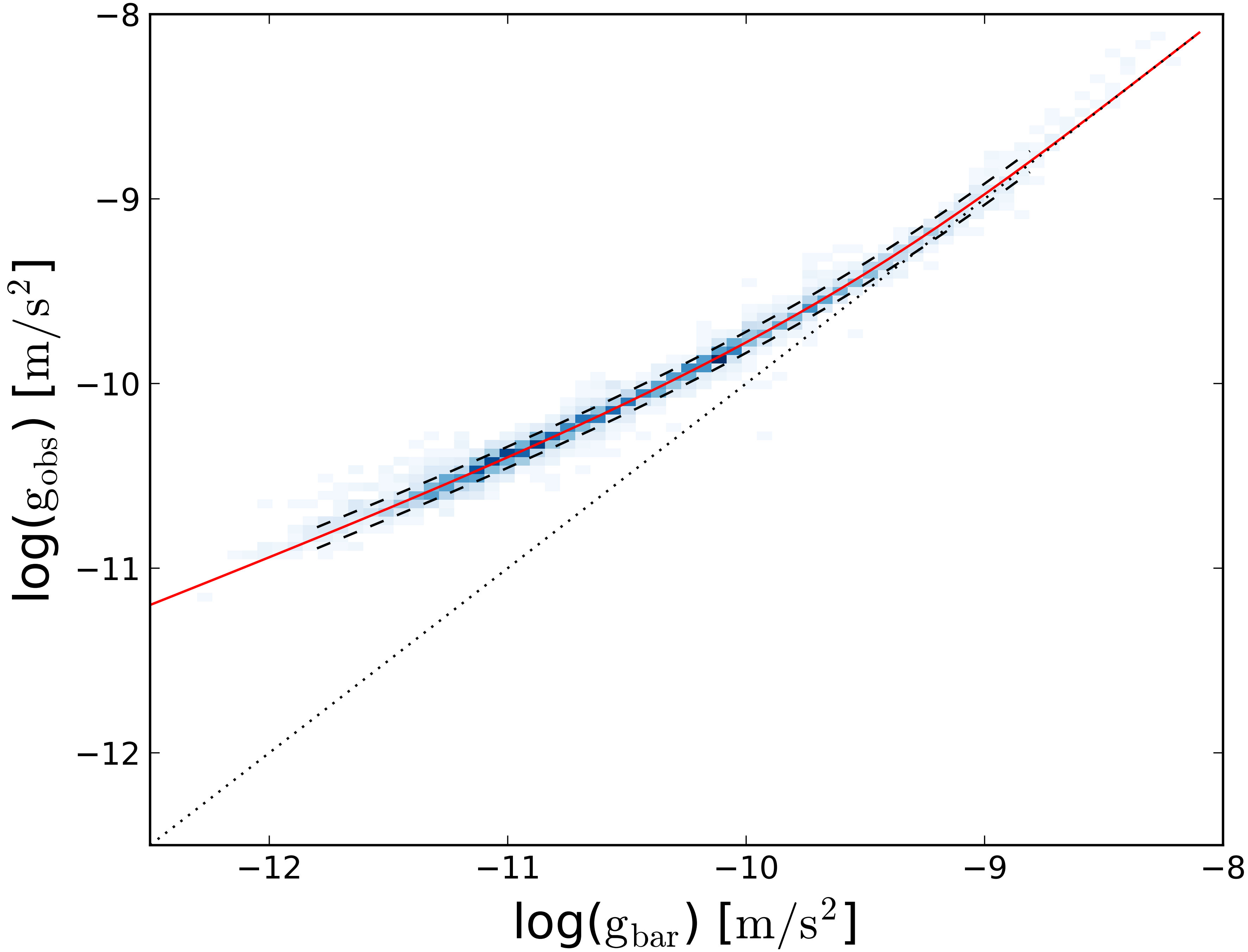

No need to vary g+, which covaries with M*/L
The data constrain one or the other; not both
(Li et al. 2018)

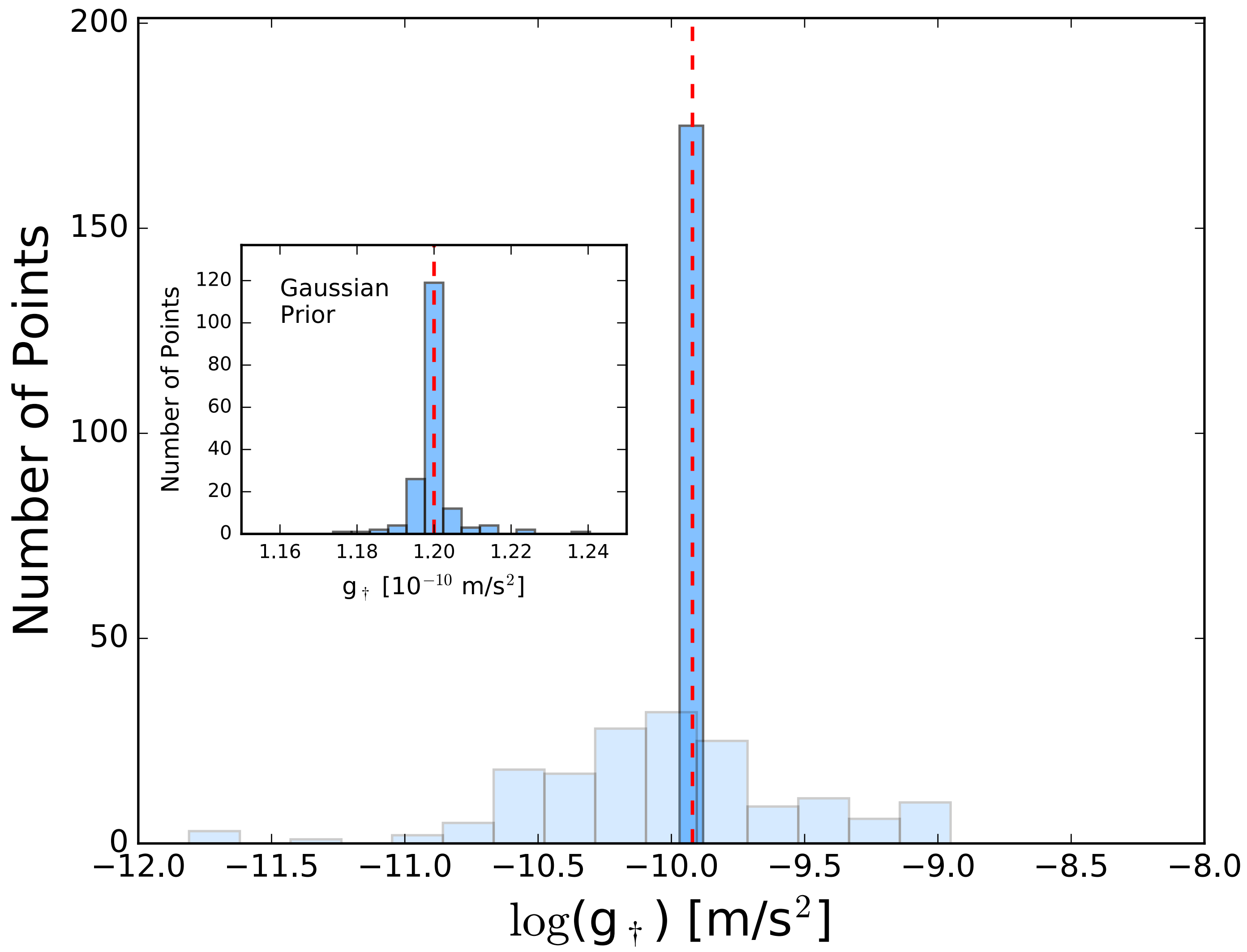

The distribution of fitted M*/L is reasonable

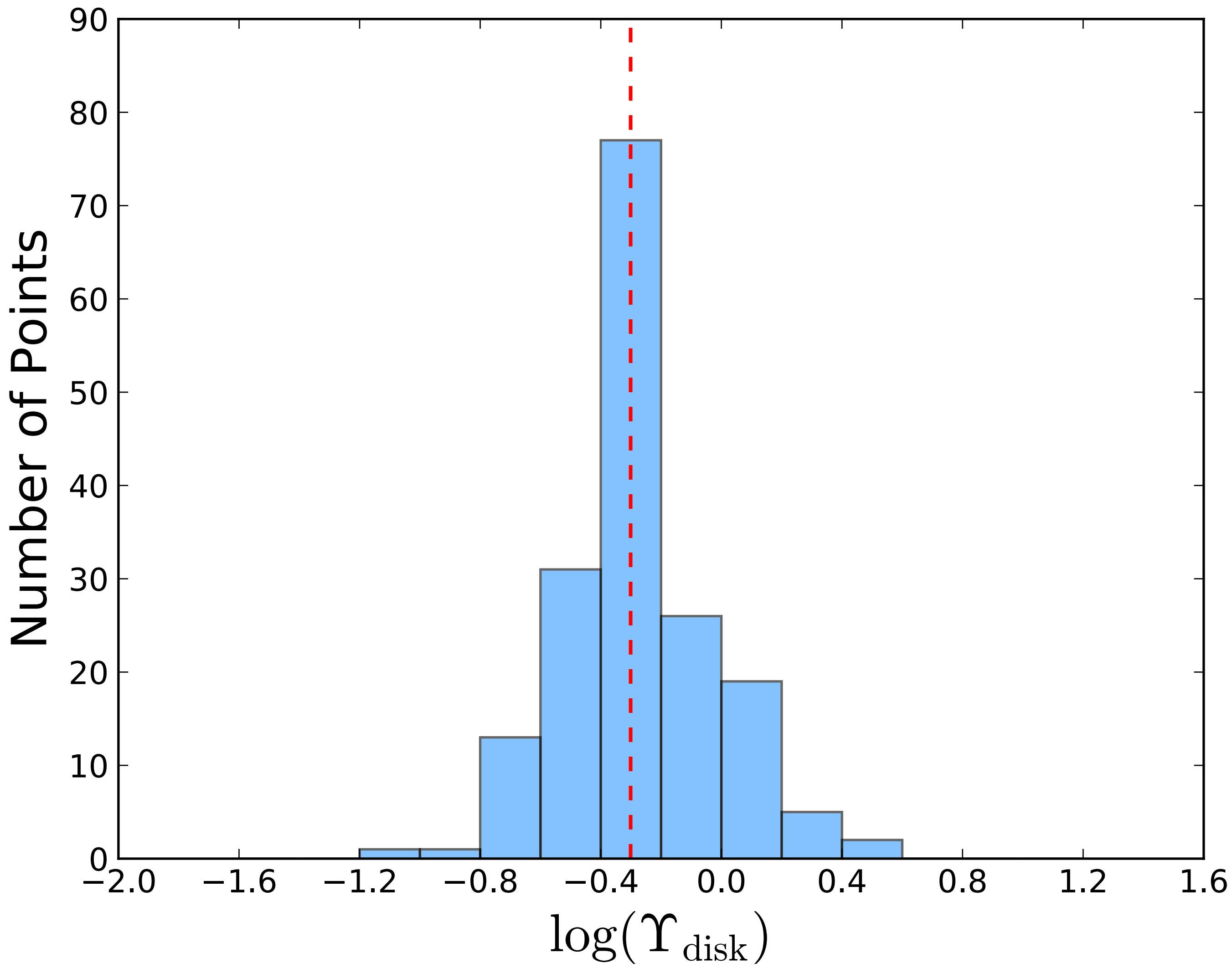

There are striking regularities in galaxy dynamics

- Flat Rotation Curves
- Baryonic Tully-Fisher Relation
- Central Density Relation
- Renzo’s Rule
- Radial Acceleration Relation